LBL-20485 c.2

Lawrence Berkeley Laboratory

UNIVERSITY OF CALIFORNIA

RECEIVED
LAWRENCE
BERKELEY LABORATORY
APR 14 1986
LIBRARY AND
DOCUMENTS SECTION

Materials & Molecular Research Division

To be presented at the Earl R. Parker Symposium
on Structure/Property Relationships,
New Orleans, LA, March 3, 1986

THE DESIGN OF TOUGH FERRITIC STEELS FOR CRYOGENIC USE

J.W. Morris, Jr.

October 1985

TWO-WEEK LOAN COPY
This is a Library Circulating Copy
which may be borrowed for two weeks.

LBL-20485 c.2

Prepared for the U.S. Department of Energy under Contract DE-AC03-76SF00098

DISCLAIMER

This document was prepared as an account of work sponsored by the United States Government. While this document is believed to contain correct information, neither the United States Government nor any agency thereof, nor the Regents of the University of California, nor any of their employees, makes any warranty, express or implied, or assumes any legal responsibility for the accuracy, completeness, or usefulness of any information, apparatus, product, or process disclosed, or represents that its use would not infringe privately owned rights. Reference herein to any specific commercial product, process, or service by its trade name, trademark, manufacturer, or otherwise, does not necessarily constitute or imply its endorsement, recommendation, or favoring by the United States Government or any agency thereof, or the Regents of the University of California. The views and opinions of authors expressed herein do not necessarily state or reflect those of the United States Government or any agency thereof or the Regents of the University of California.

THE DESIGN OF TOUGH FERRITIC STEELS FOR CRYOGENIC USE

J. W. Morris, Jr.

Materials and Molecular Research Division,
Lawrence Berkeley Laboratory
and
Department of Materials Science and Mineral Engineering,
University of California, Berkeley, California 94720

ABSTRACT

This paper describes the design of ferritic steels and weldments that combine strength and toughness at cryogenic temperatures. The alloy must have a ductile-brittle transition temperature below the intended service temperature and a high fracture toughness in the ductile mode. Its systematic design uses the microstructure-property relations that govern the transition temperature and fracture toughness to identify a suitable microstructure, and then employs the microstructure-processing relations that govern its thermal response to manipulate the microstructure into the appropriate form. The procedure is illustrated by describing the heat treatments, microstructures and properties of a variety of laboratory and commercial alloys, including conventional "9Ni" steel, the low-Ni and Fe-Mn ferritic steels that have been developed as an alternative to 9Ni, the 12Ni steels that are promising for use at 4K, and the welding procedures and ferritic filler metals that are useful for ferritic cryogenic steels.

INTRODUCTION

The design of ferritic steels for low temperature use is an appropriate topic for a symposium honoring Professor Earl Parker, for at least two reasons. First, Professor Parker was active in the field in the early 1970's and was instrumental in beginning a program of research at LBL that continues to this day [1]. Second, Professor Parker had a strong interest in the methodology of alloy design, and the development of the modern ferritic cryogenic steels offers several good examples.

The quest for good low-temperature structural alloys is largely driven by two parallel technological needs: the transportation and storage of liquified gases at temperatures near that of liquid nitrogen (77K), and the support of superconducting magnets that operate at 4K. Since both technologies employ welded structures, superior weldments are also required. There have been substantial advances in both ferritic cryogenic steels and weldments during the past fifteen years. The following paper reviews some of those advances from the perspective of alloy design.

ALLOY DESIGN

In theory, a two step procedure is sufficient to design an alloy to match a pre-selected set of engineering properties: (1) using known structure-property relations, one identifies a composition and microstructure that will have those properties; (2) using known structure-processing relations, one selects a processing sequence that will produce that microstructure. In practice neither the structure-property nor the structure-processing relations are perfectly known. Successful alloy design always requires some patience, a bit of iterative trial-and-error, and a dash of luck. But it is more and more common to find alloy design projects based on a systematic effort to identify appropriate microstructures and achieve them.

The Structure-Property Relations

While the sources of strength and toughness in ferritic steels are not fully understood, the simple relations that are diagrammed in Figure 1 suffice for most alloy design purposes. The basic relation between the fracture toughness and the temperature is shown at the upper right. The fracture toughness drops dramatically over a relatively narrow temperature range that defines the ductile-brittle transition temperature (T_B). The ductile-brittle transition is caused by a change in the fracture mode from ductile rupture to transgranular cleavage or intergranular separation. If the steel is to have high toughness at its intended service temperature, T_B must be decreased to below the service temperature and the fracture toughness in the ductile mode must be raised to an acceptable value.

The fracture toughness of a typical ductile alloy is related to its yield strength by a relation like that shown in the plot at upper right. As the yield strength increases, the fracture toughness falls. The strength-toughness characteristic is controlled by the flow properties of the matrix and by the density and efficacy of the ductile void nucleation sites. The latter are governed by the inclusion type and count, which reflect the chemical purity of the alloy. One can increase the toughness above T_B by processing the alloy to lower its strength or decrease its inclusion content.

The ductile-brittle transition can be usefully described in terms of the "Yoffee diagram" at the lower left in Figure 1. The Yoffee model is oversimple, but nonetheless contains the most important alloy design criteria in a compact form. It attributes the ductile-brittle transition to a competition between plastic deformation and brittle fracture. At a critical value of the yield stress (σ_c) the material ahead of an embedded flaw fractures in a brittle manner before blunting so that the ductile mode is preferred. As the temperature is lowered the yield strength of the alloy rises until it exceeds σ_c. The crossover point determines T_B. Since there are at least two independent brittle fracture modes, transgranular cleavage and intergranular separation, there are at least two critical stresses. The transition temperature and the brittle fracture mode are determined by the least value of σ_c.

The Yoffee diagram suggests that T_B can be decreased by lowering the alloy strength or by raising its resistance to fracture in the dominant brittle mode. While both approaches have been used successfully, the preferred tactic is to raise the resistance to brittle fracture, since high strength is a desirable characteristic of structural steel. This is done by identifying the brittle fracture mode and its relation to the microstructure. If the brittle fracture mode is intergranular, T_B can be lowered by increasing boundary cohesion, either by removing embrittling species, such as sulfur and phosphorous in typical steels, or by adding species that segregate to the boundary and improve its cohesion. If the brittle fracture mode is transgranular the alloy may be toughened by decreasing its effective grain size [4-7], the mean free path for cleavage fracture.

The Ductile-Brittle Transition in Ferritic Steels

The ferritic steels that have shown the greatest promise for structural use at low temperature are Fe-(5-12)Ni and Fe-(5-6)Mn alloys. (Fe-(10-12)Mn alloys can also be processed to have good cryogenic toughness [8], but these alloys have behavioral peculiarities that are beyond the scope of this paper.) The central problem in the development of these alloys was to identify heat treatments that suppressed T_B. Hence the most important structure-property relation was that which governs the onset of brittle fracture.

If an Fe-Ni or Fe-Mn alloy of the class identified above is tested in the as-quenched condition it fractures in the ductile mode at temperatures above a T_B that lies in the vicinity of room temperature. If the alloy has a reasonably low impurity content (sulfur and phosphorous are the most important impurity species) then the fracture mode below the ductile-brittle transition is transgranular cleavage, as shown in Figure 2. The cleavage facets are relatively flat and several microns in size, suggesting that they correspond to a particular feature of the microstructure, an "effective grain size".

In the as-quenched condition these alloys have a dislocated martensite structure that resembles the one shown in Figure 3 [9]. The overall microstructure is a hierarchy of three elements. It is built of dislocated martensite laths, which are cigar-shaped, and lie parallel to one another in "packets". (In some high nickel martensites the packets are subdivided into "blocks" of laths that differ in their etching characteristics, but this feature rarely appears in the steels of interest here). One or more martensite packets fill each prior austenite grain.

The microstructure appears fine-grained in optical or bright-field transmission electron micrographs, but is not. The laths within a given packet have a close crystallographic correspondence to one another, as evidenced by the clean diffraction pattern obtained from the interior of a packet (Figure 4 [10]). The lath boundaries are low-angle boundaries. The packet is essentially a single crystal of martensite whose crystal planes are continuous.

The alloy microstructure is reflected in its cleavage mode, which is revealed in the profile scanning fractograph in Figure 5 [9]

and the profile transmission electron micrograph in Figure 6 [11]. The cleavage facet cuts across the laths within a packet on a common {100} cleavage plane (or, occasionally, {112} plane), and branches at packet boundaries where the crystallographic orientation changes. The effective grain size in the alloy is the packet size.

To minimize the ductile-brittle transition temperature the martensite packet size should be as small as possible. The heat treatments of ferritic cryogenic steels are designed to achieve this objective.

The Structure-Processing Relation

The heat treatments that are normally used in the processing of ferritic cryogenic steels can be visualized as variations on a single elementary step in which the alloy be quenched to the lath martensite structure shown in Figure 3, and then reheated to accomplish a partial or complete reversion to the austenite phase. The Fe-Ni and Fe-Mn martensites undergo a characteristic sequence of microstructural changes as the reheat temperature is raised [12]. The four characteristic reactions are indicated in Figure 7 [3] along an isocomposition line in a schematic drawing of the Fe-rich section of the binary phase diagram. The four reactions are described below. The letters in parentheses after the each label are the symbols that are often used to designate them.

(1) Normal Tempering (t). Normal tempering occurs when the steel is held at a temperature at which the α phase is maintained. The common reactions include the precipitation and growth of carbides, dislocation polygonization and recovery, and the equilibration of point defects. Using the symbol α' to indicate fresh martensite and α_T for tempered martensite the reaction is

$$\alpha' \rightarrow \alpha_T \tag{1}$$

(2) Intercritical Tempering (T). If the alloy is reheated to a temperature just within the two-phase ($\alpha+\gamma$) region then a solute-rich γ phase precipitates while the residual α phase loses solute and tempers. Most commonly, the γ forms small islands along the lath boundaries of the martensite. Because of its small size and high solute content the austenite is retained on cooling to low temperature. The final microstructure contains a tempered martensite whose lath boundaries are decorated with austenite, as illustrated in Figure 8 [13]. The reaction is

$$\alpha' \rightarrow \alpha_T + \gamma \tag{2}$$

The precipitated austenite that forms during intercritical tempering serves two functions that are useful in the processing of ferritic cryogenic steels. The austenite getters carbon and other solutes from the martensite lattice, which softens the lattice, and it decomposes the martensite packet, which, in a somewhat subtle way that will be described below, refines the effective grain size of the steel.

(3) Intercritical Annealing (B,L,Q'). If the alloy is heated to the upper part of the two-phase region a more extensive decomposition occurs. The γ phase formed at these temperatures is relatively lean in solute and retransforms during cooling, producing a microstructure that is a mixture of tempered and fresh martensite with a small residue of austenite. The reaction is

$$\alpha' \rightarrow \alpha_T + \gamma \rightarrow \alpha_T + \alpha' + \gamma \qquad (3)$$

While intercritical annealing produces a "dual-phase" microstructure it does not significantly refine the effective grain size. The reason is that the austenite precipitated along a lath boundary has a strong tendency to retransform into the particular variant of martensite that defines the surrounding packet. Figure 9 [13] shows the microstructure of an Fe-6Ni alloy after intercritical annealing. While the microstructure appears irregular the diffraction pattern is simple. The packet is essentially a single crystal.

However, the martensite packet is chemically heterogeneous after intercritical annealing. The α_T in the final alloy is relatively lean in carbon, nickel and manganese, while the α' and the retained γ are relatively rich in alloying elements [14]. The chemical redistribution has a minor influence on the mechanical properties of the alloy but substantially affects its response to further heat treatment.

(4) Austenite Reversion (A,Q). If the alloy is heated through the $(\alpha+\gamma)$ region it reverts to the γ phase, and retransforms to α on subsequent transformation to room temperature. The reaction is

$$\alpha' \rightarrow \gamma \rightarrow \alpha' \qquad (4)$$

The microstructure that results from austenite reversion depends on the reversion temperature and holding time [16], as illustrated in Figure 10. There are two limiting cases, illustrated by the "step" and the "spike" thermal profile in the figure.

In the "step" treatment the alloy is heated into the γ field and held before quenching. While the mechanisms of reversion remain uncertain, it is clear that the reverted austenite phase is a highly defective phase that recrystallizes if held for a reasonable time at temperatures within the γ stability field. If the alloy is quenched after recrystallization but before significant grain growth the austenite grain size is small. Since the martensite packets fill or subdivide prior austenite grains, the martensite packet size is also refined. Step reversion treatments have been used for some years to refine the effective grain size and lower the ductile-brittle transition temperature of lath martensitic steels [17-20].

In the "spike" treatment the alloy is heated rapidly to accomplish the γ transformation, then immediately quenched to room temperature. The result is a dramatic refinement of the effective grain size to nearly 1μm [16]. The apparent reason for this "packet refinement" is the defective state of the austenite when it is first formed. Since recrystallization is not permitted, the defects perturb the martensitic transformation and prevent the alignment of martensite laths into well-

defined packets. The "spike" treatment is normally inapplicable to steel plate because of the rapid heating and cooling rates required. However, it is the thermal profile normally imposed during multi-pass welding, and is the basis of the recent successful development of ferritic weldments ferritic cryogenic steels [21-23].

ALLOYS AND HEAT TREATMENTS

The first successful ferritic cryogenic steel was 9Ni steel, which was developed by the International Nickel Company during the Second World War [24]. After significant advances in its metallurgy, heat treatment, and welding, 9Ni steel is still the most commonly used ferritic cryogenic steel. However, 9Ni steel suffers from two shortcomings that have encouraged the invention of new alloys: it is relatively expensive because of its high Ni content, and it becomes brittle at temperatures below 77K. The former problem led to the development of low-Ni [25-27] and Ni-free alloys [8,28-30]. The latter led to the design of alloys for potential service at 4K.

In the following we first review the compositions and heat treatment of base-plate material, beginning with 9Ni steel, and follow with a brief discussion of ferritic weld alloys and welding procedures.

9Ni Steel

A typical composition of modern 9Ni steel is, in weight percent, Fe-9Ni-1Mn-0.2Cr-0.2Si-0.06C-0.004P-0.004S. The alloy is normally processed through a "QT" thermal treatment, in which the alloy is homogenized, austenitized at approximately 800°C for 1 hour and quenched (Q), then intercritically tempered at 570-600°C for 1 hour (T). The Q treatment recrystallizes the alloy to produce a dislocated lath martensite with a reasonably small effective grain size. The T treatment tempers the martensite and causes the precipitation of 5-10 volume percent austenite along the lath boundaries.

The change in impact toughness after heat treatment is shown in Figure 10 [12]. The toughness-temperature relation is altered in two ways: the upper shelf toughness increases and the ductile-brittle transition temperature decreases. Recent research suggests that the two changes have different mechanistic origins.

The upper shelf toughness is largely controlled by the alloy strength and the density of void nucleation sites. Two microstructural changes occur during intercritical tempering to lower the alloy strength: the transformation-induced dislocations recover, and the matrix carbon segregates strongly to the austenite phase [31] where it is much less effective in strengthening. Carbides that may act as void nucleation sites also dissolve into the austenite [32]. If the alloy contains an appreciable sulfur or phosphorous content its toughness is also lowered by intergranular separation that may contribute intergranular fracture or nucleate ductile voids. Sulfur and phosphorous are gettered into the austenite during its precipitation [33].

The decrease in alloy strength that accompanies the intercritical tempering treatment decreases the ductile-brittle transition tem-

perature somewhat, but it is clear that the major part of the decrease in T_B is due to the presence of precipitated austenite [34]. The mechanism by which the austenite lowers T_B has been a matter of discussion. Possibly the earliest suggestion was the "blunting" effect of the relatively ductile austenite phase. This mechanism was ruled out by the demonstration [13] that the precipitated austenite transforms to martensite ahead of the crack tip, and is not available to blunt a fracture. Moreover, a study of the mechanical properties of an austenitic alloy made to match the composition of the precipitated austenite [35] showed that this material is brittle. A second suggested mechanism was "transformation toughening" by the martensitic transformation of the austenite. This possibility is ruled out by the fact that the decrease in T_B is essentially independent of the austenite fraction, and is most pronounced when the precipitated austenite fraction is relatively small [11,15].

The interpretation that appears to account for at least most of the austenite effect in 9Ni and related cryogenic steels is based on the crystallography of the re-transformed austenite [10,11]. Figure 11 [11] illustrates the crystallography of the transformation of precipitated austenite under load. While the thermal transformation of precipitated austenite in tempered steel leads to a martensite particle that has the crystallographic variant of the surrounding packet, the transformation of an austenite particle under load usually creates a martensite with a different variant. By Le Chatelier's Principle the variant chosen is the one most compatible with the applied load. It follows that the transformation of precipitated austenite under load decomposes the martensite packet by introducing islands of different crystallographic orientation. The effect is to inhibit cleavage fracture and lower the ductile-brittle transition temperature.

To toughen the alloy by this mechanism the precipitated austenite must be thermally stable and densely distributed through the microstructure. The thermal stability of the precipitated austenite is achieved by strong solute segregation of Ni and C at the relatively low tempering temperature [14,15] and by the small size of the precipitated particles [31] at the relatively short tempering times employed. The dense distribution (apparent in Figure 8) is due to the high nickel content and the presence of a high density of lath boundary sites. If the alloy is tempered for long times the austenite fraction increases, but the particles coarsen and their carbon content decreases. The thermal stability of the austenite is lost and the ductile-brittle transition temperature increases dramatically [15].

Each of the minor alloy additions to commercial 9Ni steel also plays a role in its behavior. The Mn and Cr additions improve the response to intercritical annealing; Mn is an austenite stabilizer that diffuses more rapidly than Ni and promotes the precipitation of austenite during the early stages of tempering while Cr inhibits precipitation along the prior austenite grain boundaries.

Low-Nickel Alloys

Given that Ni is the costly alloy addition to 9Ni steel there is an obvious economic incentive to reduce the nickel content. For this

reason cryogenic steels of (5-6)Ni content were produced by Nippon Steel [25,26] and by Armco Steel [36]. More recently a 3.5Ni cryogenic steel was developed by Nippon Kokan [27]. The most thoroughly researched of these alloys is the Nippon 5.5Ni (typical composition: Fe-5.9Ni-1.2Mn-0.7Cr-0.2Mo-0.2Si-0.06C-0.01S-0.08P), which can serve as an example.

It is reasonable to expect good cryogenic properties if one reproduces the microstructure of 9Ni steel in an alloy of lower Ni content. Hence the central problem is the design of appropriate heat treatments for the low-Ni alloys. In particular, their microstructures should replicate the dense distribution of stable austenite precipitates along the lath boundaries. However, if a 6Ni steel is given a 1-2 hr. intercritical temper to mimic the treatment of 9Ni steel very little austenite is formed, and that which does appear is lean in solute and thermally unstable [11]. The fraction of austenite can be raised by increasing the tempering time; if Nippon 5.5Ni is tempered for 100 hrs. at 600°C it develops about 8 volume percent of stable precipitated austenite. But this austenite is blocky and dispersed in the microstructure and does not effectively disrupt the crystallographic alignment within the martensite packets (Figure 12). Both short and lengthy tempers leave the ductile-brittle transition well above 77K (Figure 13).

The problem of reproducing the 9Ni microstructure in a (5-6)Ni alloy was solved by the development of the so-called "QLT" heat treatment. In the case of the Nippon 5.5Ni steel the heat treatment sequence is: austenitization at 800°C for 1 hour, water quench (Q); intercritically anneal at 670°C for 1 hour, water quench (L); intercritically temper at 600°C for 1 hour, water quench. Both the microstructure and the strength-toughness combination of QLT 5.5Ni at 77K are similar to those of 9Ni steel in the QT condition.

The microstructural changes that occur during the QLT treatment are diagrammed in Figure 14. The Q treatment establishes a dislocated martensite structure with a small prior austenite grain size. During the L step the alloy decomposes to a mixture of austenite and tempered martensite. Because of the high temperature of the L treatment most of the austenite reverts to martensite on cooling, and since each of the austenite islands tends to transform to the crystallographic variant of its surrounding martensite packet, T_B remains high (Figure 13). However, the L treatment does induce a chemical decomposition of the alloy. The austenite formed at 670°C contains approximately 8Ni and 3.5Mn [14], and retains this composition when it re-transforms. The resulting microstructure is a fine mixture of low-alloy laths (the original martensite) and high-alloy laths (the fresh martensite).

During the intercritical temper that completes the QLT treatment austenite nucleates readily along the boundaries of the high-alloy laths, which behave essentially as if they were 9Ni steel. The result is a dense distribution of stable precipitated austenite. Since the high-alloy lath boundaries are dense within the martensite packets, this austenite effectively decomposes the packets (Figure 15) and substantially lowers T_B (Figure 13).

A similar approach was used in the design of the NKK 3.5Ni steel [27]. However, in this case the lower Ni content makes it more

difficult to assemble high-Ni laths that will form stable austenite on tempering. The successful heat treatment is designated QQ'Q''T, and involves two successive intercritical anneals, the first at a relatively high temperature to form laths of intermediate Ni content and the second at a lower temperature to form high-Ni laths within these. The final temper causes the precipitation of a dense, stable precipitated austenite.

Fe-Mn Steels

If it is true that the ductile-brittle transition of lath martensitic steels is controlled by the microstructure, as the Fe-Ni data appears to show, then it should be possible to achieve a good combination of cryogenic strength and toughness in any alloy that can be processed into the desirable microstructure. This point was demonstrated by the successful design of ferritic Fe-Mn cryogenic steels that contain no nickel at all [28-30].

Manganese is an austenite-stabilizing element. The Fe-rich side of the binary phase diagram resembles that of the Fe-Ni diagram. However, the kinetic diagram (Figure 16) shows that the hexagonal, ε-martensite phase competes with α' martensite at Mn contents greater than about 10 weight percent. The intrusion of ε-martensite complicates the design of suitable heat treatments since the ε perturbs the phase transformation behavior of any element of the microstructure whose Mn content approaches 10% [8]. The Mn alloys also appear more susceptible to intergranular embrittlement than the Ni alloys [8].

Microstructures that resemble those of the Fe-Ni cryogenic steels have been achieved in research alloys by lowering the Mn content to 5-6 weight percent and employing careful multi-step heat treatments. The first successful effort of this type [28] employed a four-step thermal cycle treatment (the "2B" treatment discussed below) to refine the grain size of a Fe-5Mn alloy prior to intercritical tempering. As shown in Figure 17, 2BT-treated Fe-5Mn has a microstructure that resembles that of QLT-treated 5.5Ni steel, and has competitive strength-toughness properties (Figure 18). Similar microstructures and properties have since been obtained in low-P 6Mn steel using a modified QLT treatment [29-30].

12Ni Steel

Recent developments in superconducting magnet technology for magnetic fusion energy and related applications has created a need for high strength structural alloys that remain tough in liquid helium at 4K. The alloys that are most promising for those applications are recently-developed austenitic cryogenic steels [37]. But it has also been shown that ferritic steels can be processed to have good toughness at 4K [19-20,38].

The available data suggests that austenite precipitation by itself is not sufficient to suppress the ductile-brittle transition to 4K. The best of the alloys developed to date use thermal cycling treatments to refine the packet size. The grain refinement is achieved by the step heat treatment diagrammed in Figure 10. The alloy is heated

into the austenite field and held to permit recrystallization before quenching. Austenite reversion treatments of this type have been known and used in research alloys for some years [17,18]. However, the recrystallization treatment alone is not sufficient to decrease T_B to below 4K. Even repeated recrystallization cycles leave the effective grain size of an Fe-Ni steel near 10μm.

The first successful ferritic alloy for 4K service was an Fe-12Ni-0.25Ti alloy processed through the "2B" treatment that is diagrammed in Figure 19. In this treatment austenite reversion steps (A) are alternated with intercritical anneals in the sequence (ABAB). The intercritical anneal decomposes the structure and increases the efficiency of the austenite reversion [20]. Since the alloy contains Ti to getter carbon, the upper shelf toughness is naturally high. The alloy does not require tempering after heat treatment. The "2B" treatment of 12Ni-0.25Ti produces a very fine grain size whose strength-toughness combination at 4K is equivalent to that of the better stainless steels (Figure 20).

Further research on grain-refining heat treatments clarified the role of the intercritical anneal in preparing the microstructure for grain refinement after reversion. This research led to the "2K" treatment (Figure 21) in which the alloy is heated to the intercritical temperature, held, and then heated directly to the austenite field [39]. The intent is to limit recrystallization to the tempered martensite phase to achieve a finer austenite grain size. A twice-repeated cycle of this type raises the strength-toughness combination of 12Ni steel above the 4K trend band for conventional stainless steels, as shown in Figure 19. However, examination of the fracture surface of 2K-treated 12Ni steel shows that the fracture is partly by cleavage. It should, therefore, be possible to attain further improvements in the 4K toughness of ferritic steel.

In addition to potential applications in superconducting magnets, alloys treated by the "2B" and similar thermal treatments have been used by NASA to develop high-strength, dimensionally stable steels for use in aerodynamic models for cryogenic wind tunnels.

DESIGN OF FERRITIC WELDMENTS FOR FERRITIC CRYOGENIC STEELS

Many of the most important applications of ferritic cryogenic steels are in welded structures. The properties of the weldment and heat affected zone must approach those of the base plate or the structure must be designed to the poorer properties of the weld. The best weldment would be made with an alloy that essentially duplicates the base plate. However, the base plate properties are established by careful heat treatment, and it is not usually possible to apply post-weld heat treatments to the weld.

The ferritic welds that have the best cryogenic properties utilize the welding process itself to heat treat the weld and heat-affected zone. In multi-pass welding each weld pass imposes a thermal cycle on the material in its immediate surroundings that resembles the "spike" treatment shown in Figure 10. Figure 22 shows the result of a weld pass on a 12Ni steel that was overaged to create a large initial

grain size, and then embrittled to induce intergranular fracture at 77K [39]. The material near the fusion line is coarse and fractures in an intergranular mode, as does the material in the base plate and outer part of the heat-affected zone. However, there is a band of material in the inner part of the heat-affected zone that is grain-refined and ductile. This band of material has received a rapid thermal cycle that misorients adjacent laths and refines the packet size.

If the weld material is laid down in a multi-pass process controlled so that each element of the weld deposit and heat-affected zone receives rapid thermal cycles from subsequent weld passes then the weldment and heat-affected zone have a small effective grain size. If, in addition, the weld metal has high purity and the welding procedure retains cleanliness, as a gas-tungsten arc (GTA) procedure usually does, then the ductile-brittle transition in the weld zone is suppressed to very low temperature.

However, many of the ferritic cryogenic steels contain carbon. As discussed above in connection with the toughness of 9Ni steel, even if the alloy is ductile its fracture toughness remains low unless the carbon and carbides are gettered from the matrix. A well-designed multi-pass GTA process accomplishes this in a metallurgically interesting way [39]. If a grain-refined 9Ni steel is given a second thermal cycle into the two-phase region, with a peak temperature near 600°C, carbon is gathered into thin carbides along the lath boundaries. The matrix hardness decreases and the upper shelf toughness increases dramatically. The result is a weld zone that contains no precipitated austenite, but nonetheless has both a low ductile-brittle transition temperature and a high fracture toughness.

Appropriate gas-tungsten-arc (GTA) welding techniques were developed some years ago in a joint project between Kobe Steel and Nippon Kokan to weld 9Ni steel for use at 77K and above [21,22]. A suitable modification of this process has been shown to yield weldments that have exceptional toughness at 4K [40].

The viability of the rapid thermal cycle, or multipass welding scheme is perhaps best illustrated by the compact-tension fracture toughness sample shown in Figure 23 [31]. This sample was cut from a plate that was built up entirely of an 11Ni weld metal (manufactured by Kobe Steel, Ltd.) using a multipass GTA welding process. The plate is hence entirely weld metal, and yet had a fracture toughness above 100 $ksi \cdot in^{1/2}$ at 4K. Since there were flaws in the weldment that appear as fairly large brittle regions in the fracture surface, improved welding practice will almost certainly produce a substantially higher toughness.

CONCLUSION

The body of this paper documents substantial advances in the development of ferritic steels and weldments for use at cryogenic temperatures. While it is not true that such steels were, or could be, designed from first principles, their development was firmly grounded on knowledge of the microstructural sources of the ductile-brittle transition, and was achieved by intentionally manipulating the microstructure to impart good strength-toughness combinations. As such, these alloys

are realized examples of the systematic alloy design Professor Parker espoused.

ACKNOWLEDGMENT

This work was supported by the Director, Office of Basic Energy Sciences, Materials Science Division of the United States Department of Energy under contract DE-AC03-76SF00098.

REFERENCES

1. V.F. Zackay, E.R. Parker, G. Thomas and J.W. Morris, Jr., Mat. Sci. Eng., **16**, 201 (1974)

2. J.W. Morris, Jr., in Proceedings, International Conference on Phase Transformations, Chania, Crete, 1984, T. Tsakalakos, ed., Plenum, London, 1985, p.211

3. A.H. Cottrell, Trans. AIME, **212**, 192 (1958)

4. N.S. Stoloff, in Fracture, H. Liebowitz, ed., Academic Press, N.Y. (1969), vol.6, p.7

5. R.A. Grange, Trans. ASM, **59**, 26 (1966)

6. J.D. Bolton, E.R. Petty and G.B. Allen, Met. Trans., **2**, 2915 (1971)

7. M. Ogasawara, M. Iino and H. Mimura, Trans. JIM, **13**, 6 (1972)

8. S.K. Hwang and J.W. Morris, Jr., Met. Trans., **11A**, 1197 (1980)

9. Y.H. Kim, PhD Thesis, Dept. Materials Science and Mineral Engineering, Univ. California, Berkeley, June, 1985 (LBL Rept. 19962)

10. J.W. Morris, Jr., C.K. Syn, J.I.Kim and B. Fultz, in Proceedings, International Conference on Martensitic Transformations, MIT, 1979, W. Owen, ed., MIT Press, Cambridge, Mass., 1980, p. 573

11. J.I. Kim, C.K. Syn and J.W. Morris, Jr., Met. Trans., **14A**, 93 (1983)

12. J.W. Morris, Jr., J.I. Kim and C.K. Syn, in Advances in Metal Processing, J. Burke, R. Mehrabian and V. Weiss, eds., Plenum Press, New York, 1981, p. 173

13. C.K. Syn, B. Fultz and J.W. Morris, Jr., Met. Trans., **9A**, 1635 (1978)

14. J.I. Kim and J.W. Morris, Jr., Met. Trans., **12A**, 1957 (1981)

15. B. Fultz, J.I. Kim, Y.H. Kim, H.J. Kim, G.O. Fior and J.W. Morris, Jr., Met. Trans. (in press)

16. H.J. Kim and J.W. Morris, Jr., Met. Trans. (in press)

17. L.F. Porter and D.S. Dabkowski, in Ultrafine Grain Metals, V. Weiss, ed., Syracuse Univ. Press, 1972, p.113

18. G. Saul, J.A. Robertson and A.M. Adair, Met. Trans., **1A**, 113 (1970)

19. S. Jin, J.W. Morris, Jr. and V.F. Zackay, Met. Trans., **6A**, 141 (1975)

20. J.W. Morris, Jr., S. Jin and C.K. Syn, Trans. JIM, **17**(suppl.), 393 (1976)

21. "Automatic TIG Welding 9% Nickel Steels with Matching Ferritic Consumable Wire", Kobe Steel Co., Welding Electrode Div., Technical Report, May, 1974

22. "Matching Ferritic Consumable Welding of 9% Nickel Steel to Enhance Safety and Economy. Practicality of Ferritic Filler for Welding 9% Nickel Plates", Nippon Kokan KK and Kobe Steel Co. (presentation), AWS 61st Annual Meeting, Session 22 (1980)

23. H.J. Kim, PhD Thesis, Dept. Materials Science and Mineral Engineering, Univ. California, Berkeley, 1982 (LBL Rept. 14748)

24. G.R. Brophy and A.J. Miller, Trans. ASM, **41**, 1185 (1949)

25. S. Nagashima, T. Ooka, S. Sekino, H. Mimura, T. Fujishima, S. Yano and H. Sakurai, Trans. ISIJ, **11**, 402 (1971)

26. S. Nagashima, T. Ooka, S. Sekino, H. Mimura, T. Fujishima, S. Yano and H. Sakurai, Tetsu-to-Hagane, **58**, 128 (1972)

27. M. Niikura, Nippon Kokan K.K., Kawasaki, Japan, Private Communication

28. M. Niikura and J.W. Morris, Jr., Met. Trans., **11A**, 1531 (1980)

29. M. Murakami, K. Shibata, T. Fujita and K. Nagai, Trans. ISIJ, **21**, 177 (1981)

30. M. Murakami, K. Shibata and T. Fujita, in Proceedings, International Cryogenic Materials Conference, Kobe, Japan, 1982, K. Tachikawa and A. Clark, eds., Butterworths, London, 1983 p. 356

31. B. Fultz and J.W. Morris, Jr., Met. Trans., (in press)

32. J.I. Kim and J.W. Morris, Jr., Met. Trans., **11A**, 1401 (1979)

33. K.J. Kim and L.H. Schwartz, Mat. Sci. Eng., **33**, 5 (1978)

34. C.W. Marshall, R.F. Heheman and A.R. Troiano, Trans. ASM, **55**, 135 (1962)

35. J.I. Kim, H.J. Kim and J.W. Morris, Jr., Met. Trans., **15A**, 2213 (1984)

36. G.L. Swales and A.G. Haynes, Metals Progress, June, 1975, p.43

37. J.W. Morris, Jr., Adv. Cryogenic Eng., (in press)

38. H.J. Kim and J.W.Morris, Jr., Unpublished Research

39. H.J. Kim, H. Shin and J.W. Morris, Jr., in Proceedings, International Cryogenic Materials Conference, Kobe, Japan, 1982, K. Tachikawa and A. Clark, eds., Butterworths, London, 1983 p. 129

40. H.J. Kim and J.W. Morris, Jr., Welding Journal, 62, 210s (1983)

FRACTURE BEHAVIOR: STRUCTURAL ALLOYS

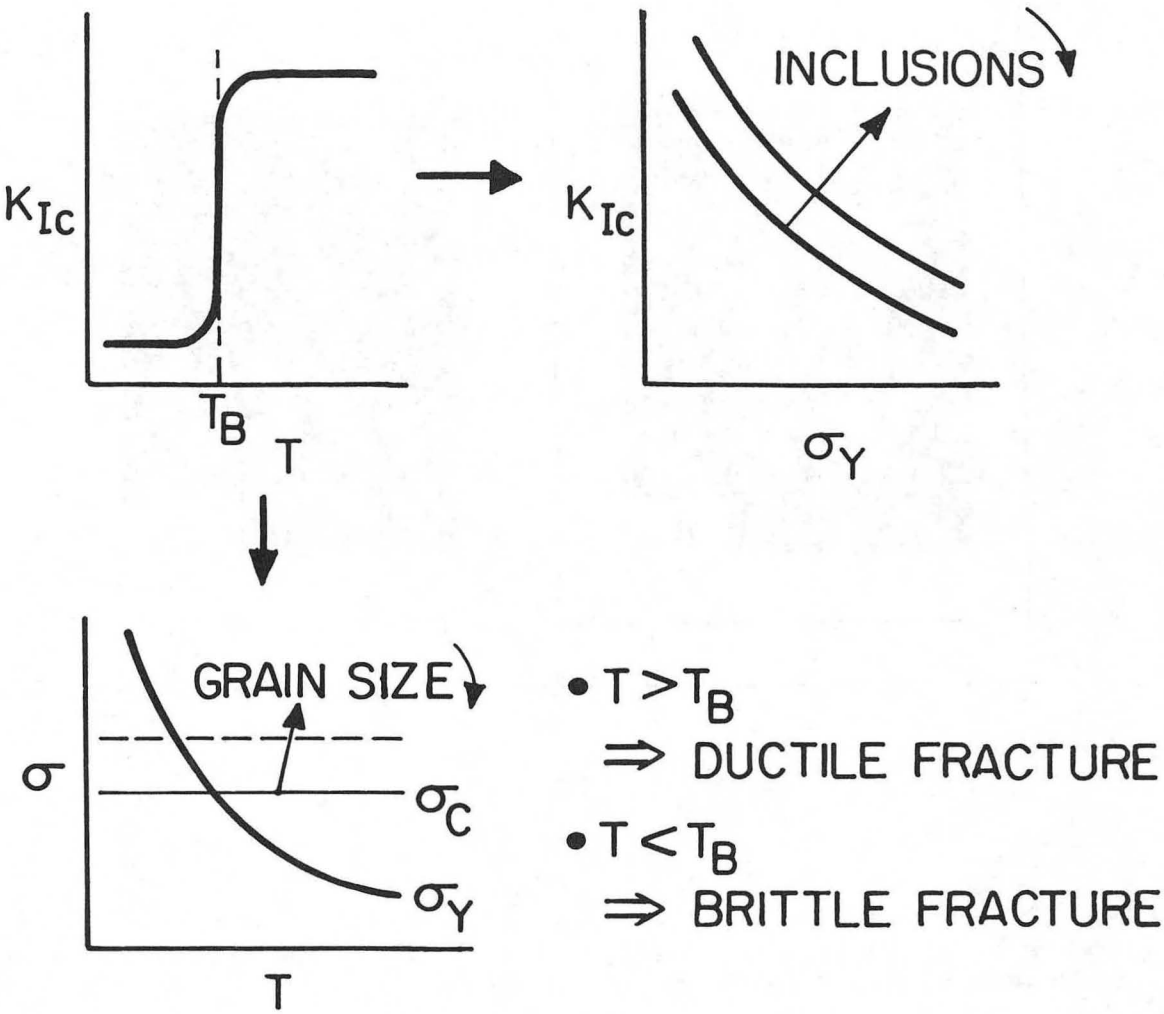

XBL 844-6932

1. Schematic presentation of the strength-toughness relations for ferritic steel.

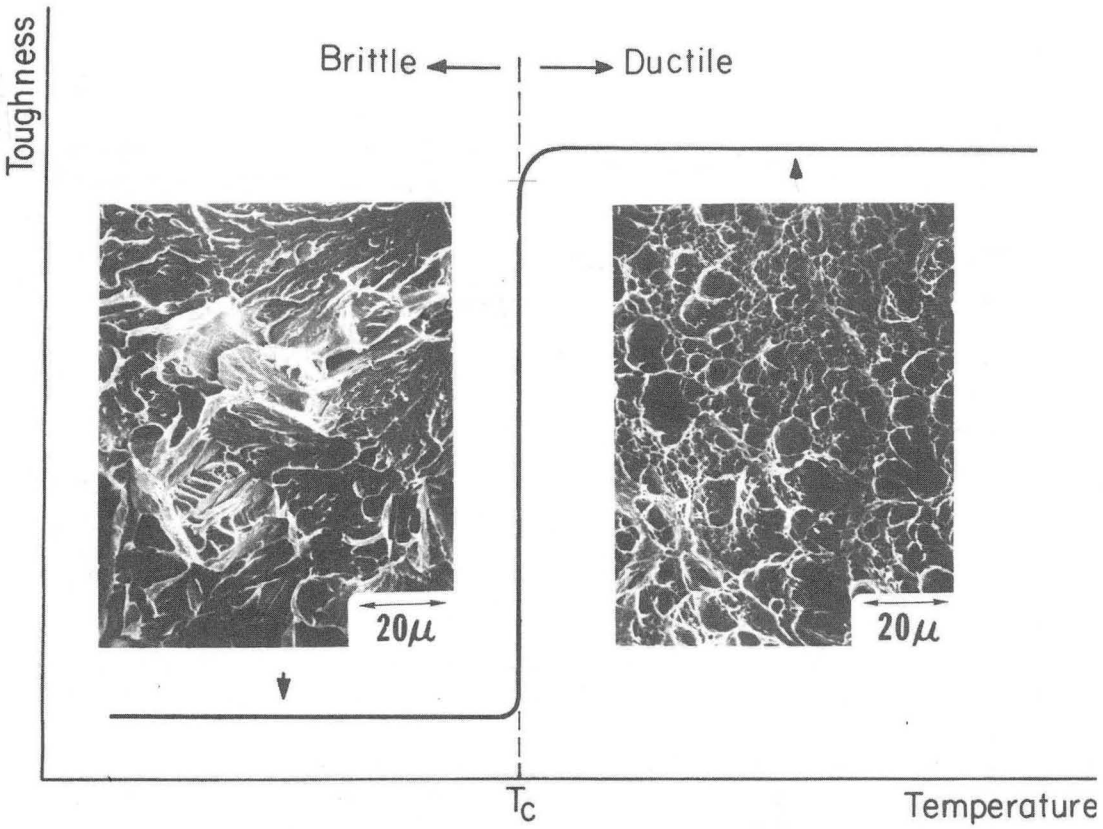

XBB 800-14845

2. Scanning electron micrographs illustrating the transition from ductile fracture to cleavage in ferritic steel.

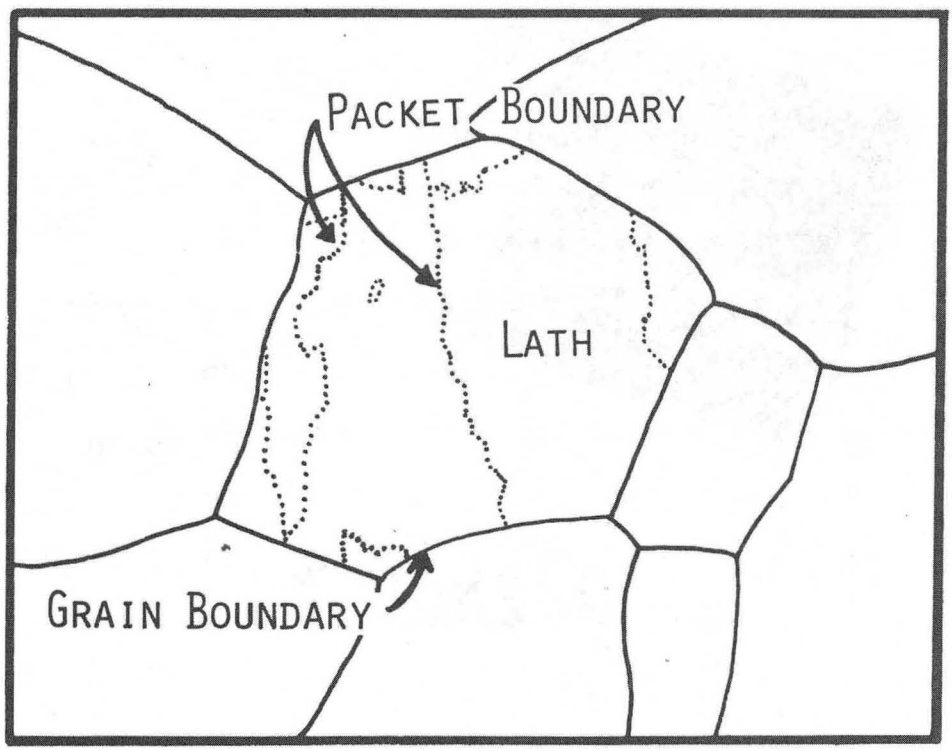

XBB 851-479

3. Optical micrograph and schematic drawing showing the prior austenite grains, martensite packets, and martensite laths in 5.5Ni steel in the as-quenched condition.

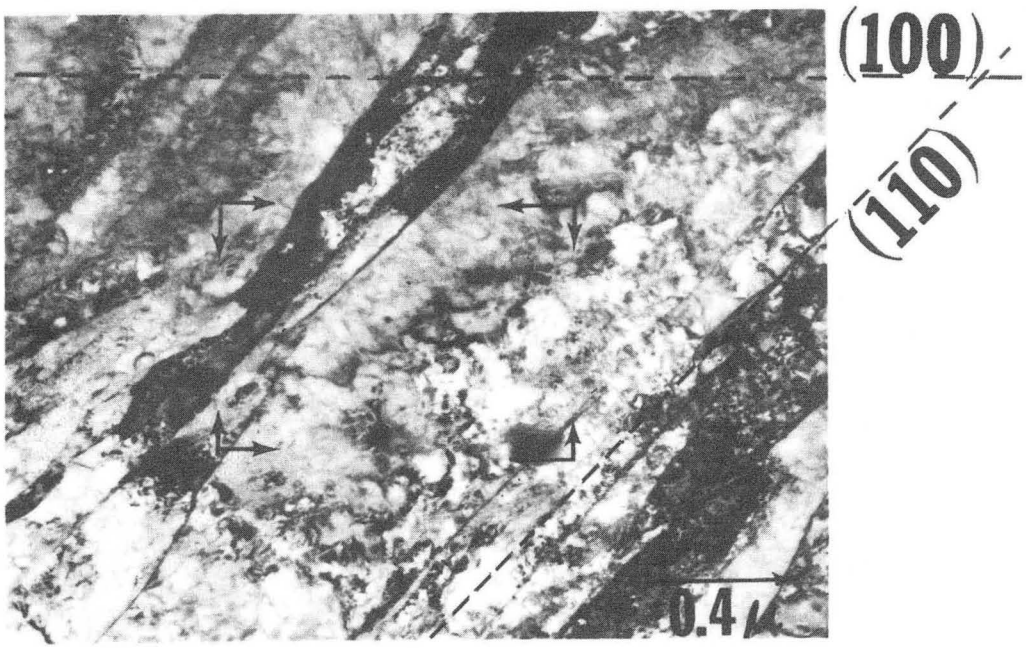

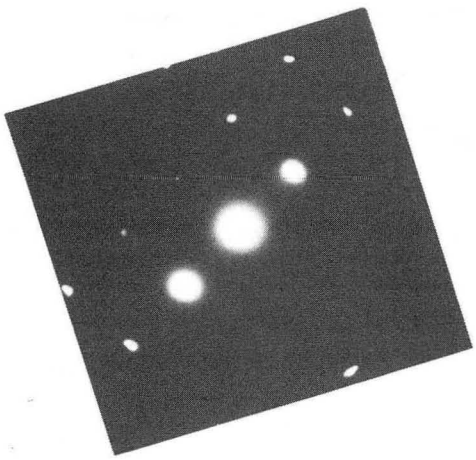

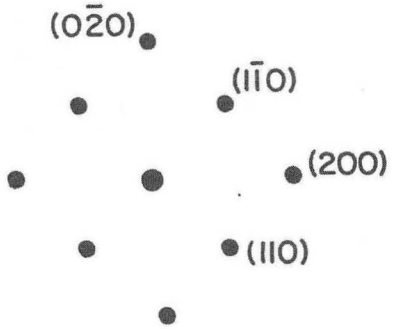

[001] martensite

QUENCHED

XBB 796-7884

4. Transmission electron micrograph of 5.5Ni steel in the as-quenched condition showing the microstructure and diffraction pattern. Example {100} and {110} planes are indicated in the micrograph.

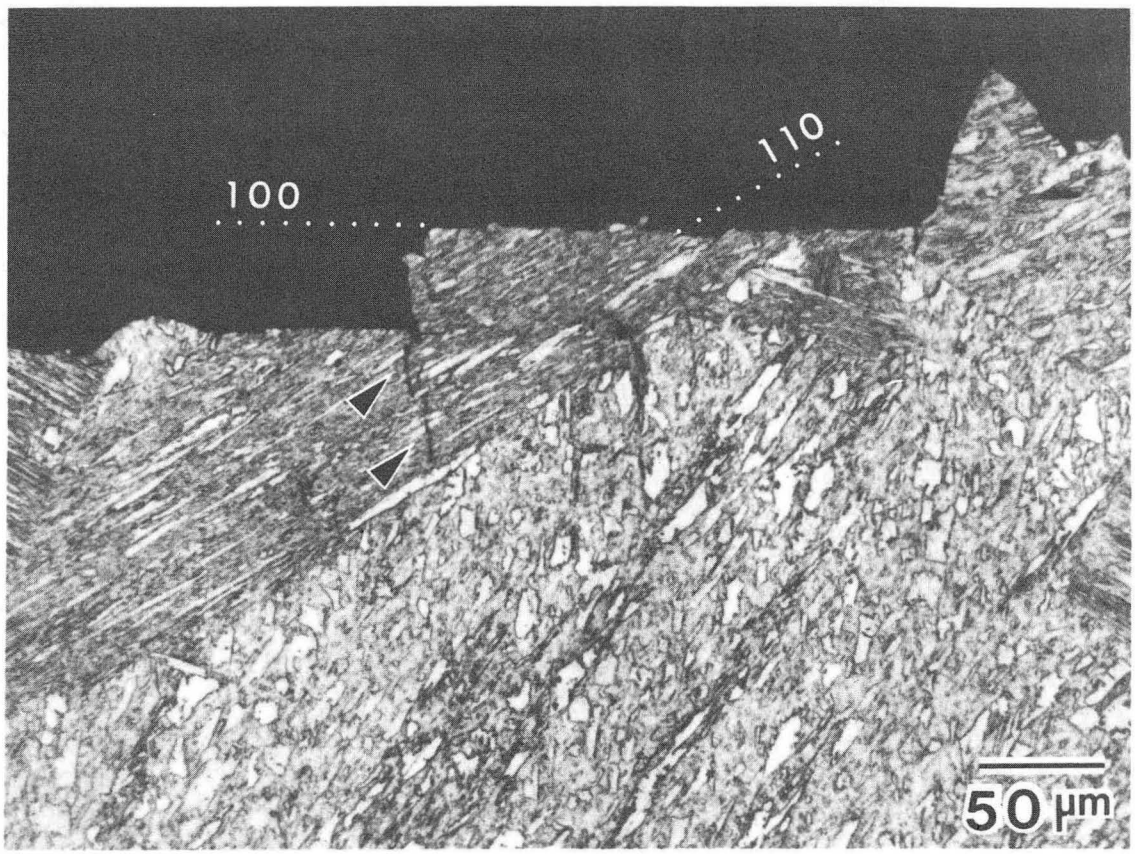

XBB 840-9676

5. Profile optical fractograph showing cleavage fracture in 5.5Ni steel broken at 77K. The side surface has been etched to reveal the cleavage across the packet on {100} planes.

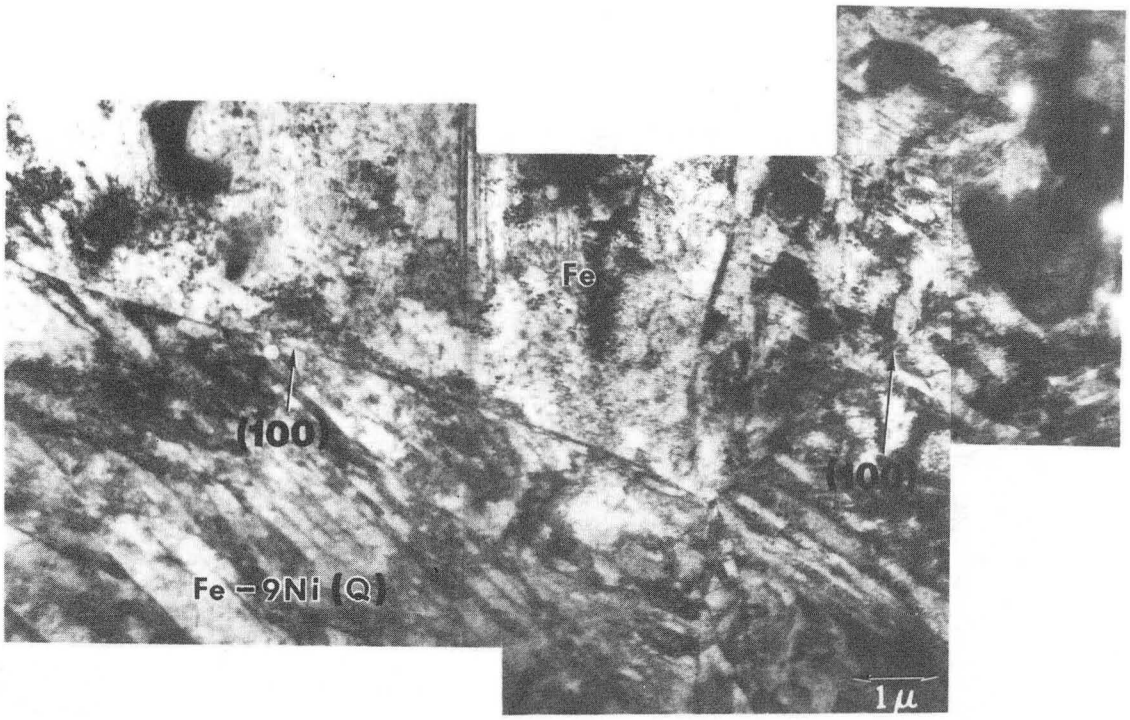

XBB 812-1672

6. Profile transmission electron fractograph showing cleavage fracture in 9Ni steel broken at 77K. The fracture surface is shown in the center of the figure. The upper part of the figure is Fe plating. The figure shows cleavage crack propagation along {100} planes. The crack branches at packet boundaries.

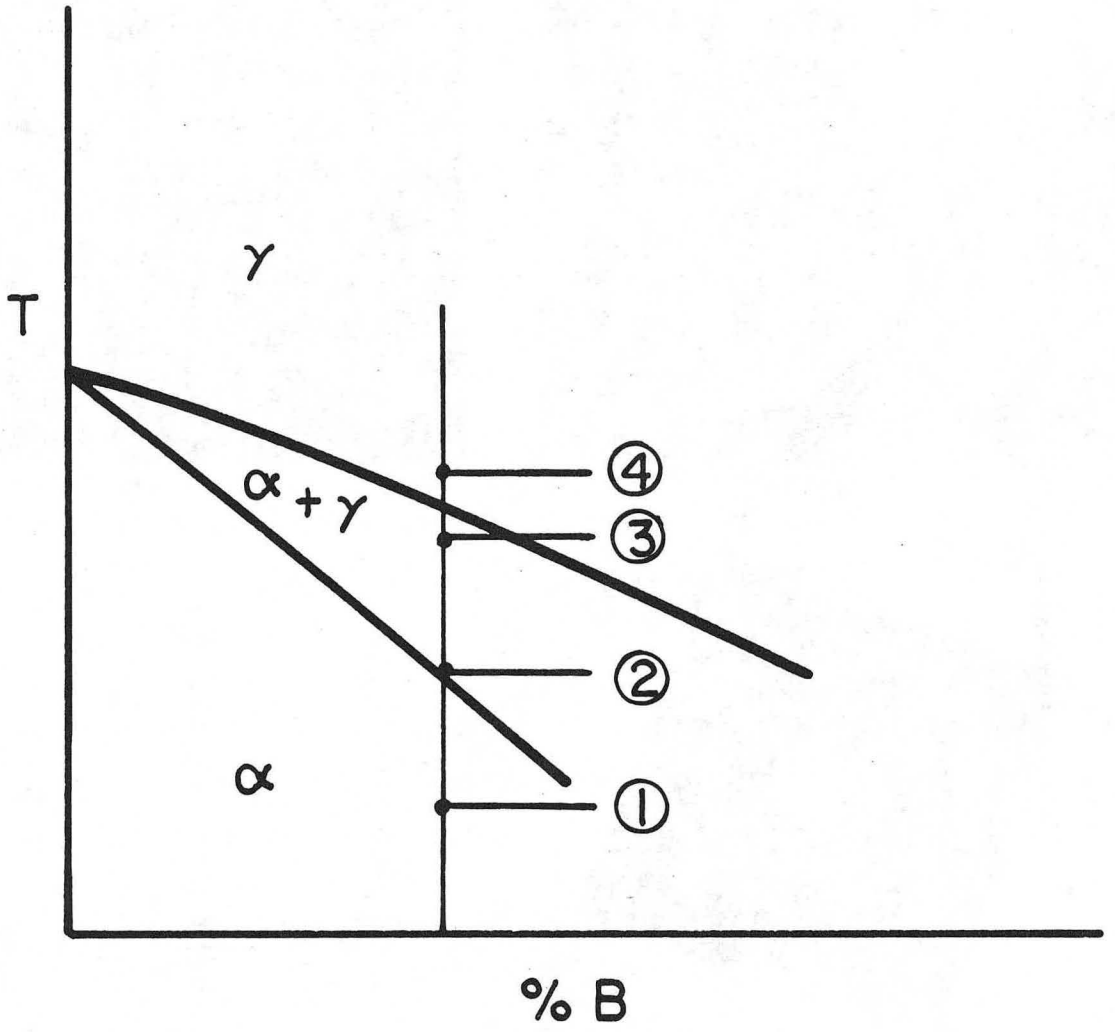

XBL796-6415

7. Schematic drawing of a section of the Fe-rich side of the Fe-Ni phase diagram with heat treatment temperatures indicated.

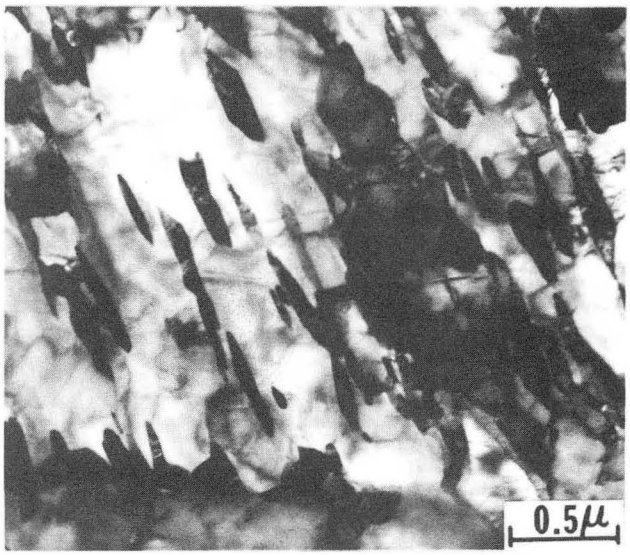

(a)

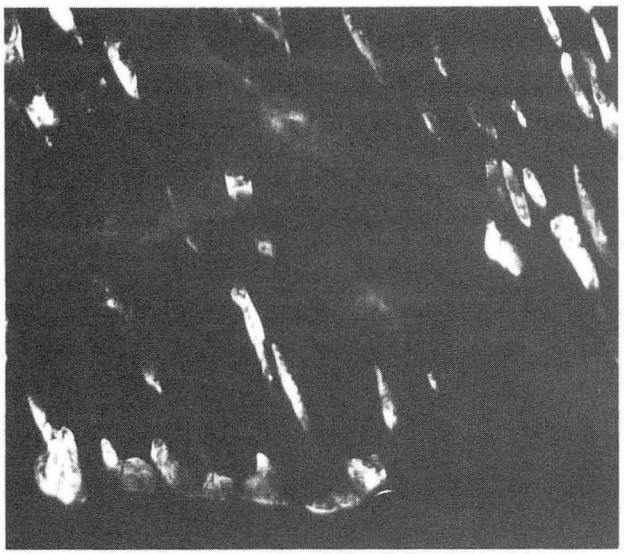

(b)

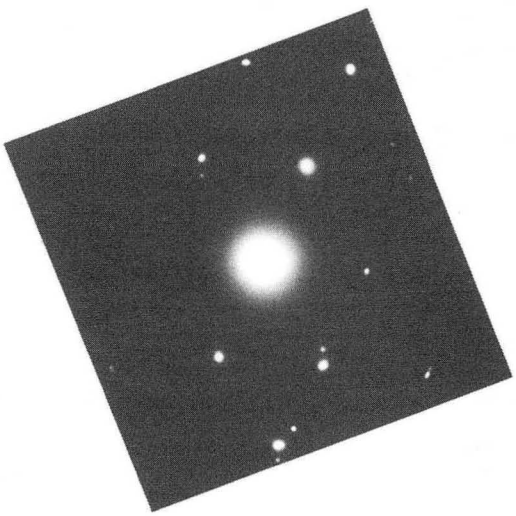

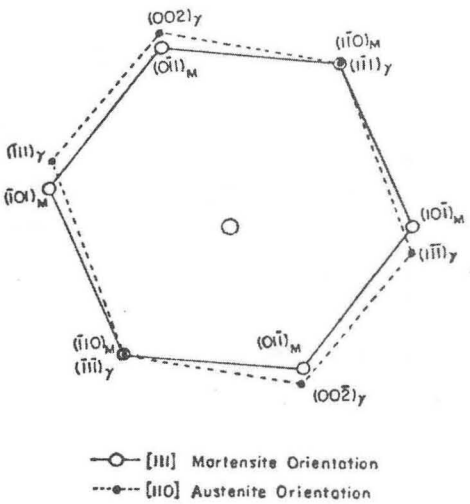

(c)

XBB 783-3328

8. Transmission electron micrographs of precipitated austenite in 9Ni steel in the QT condition: (a) bright field; (b) dark field taken from the $(00\bar{2})_\gamma$ diffraction spot in (c).

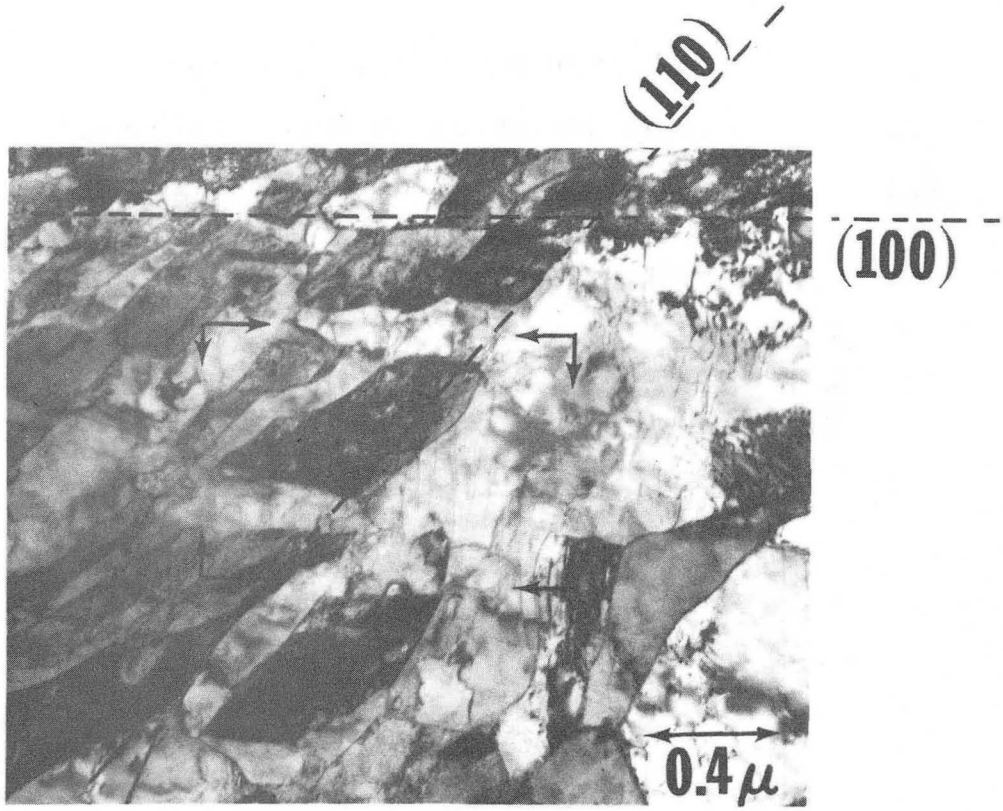

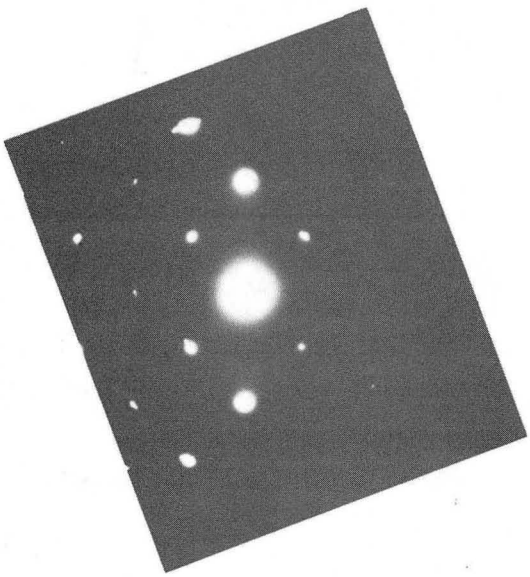

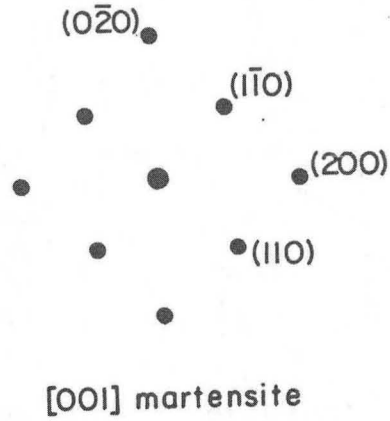

INTERCRITICALLY ANNEALED

XBB 796-7885

9. Transmission electron micrograph of 5.5Ni steel after intercritical annealing, showing (100) and (110) planes common to a packet.

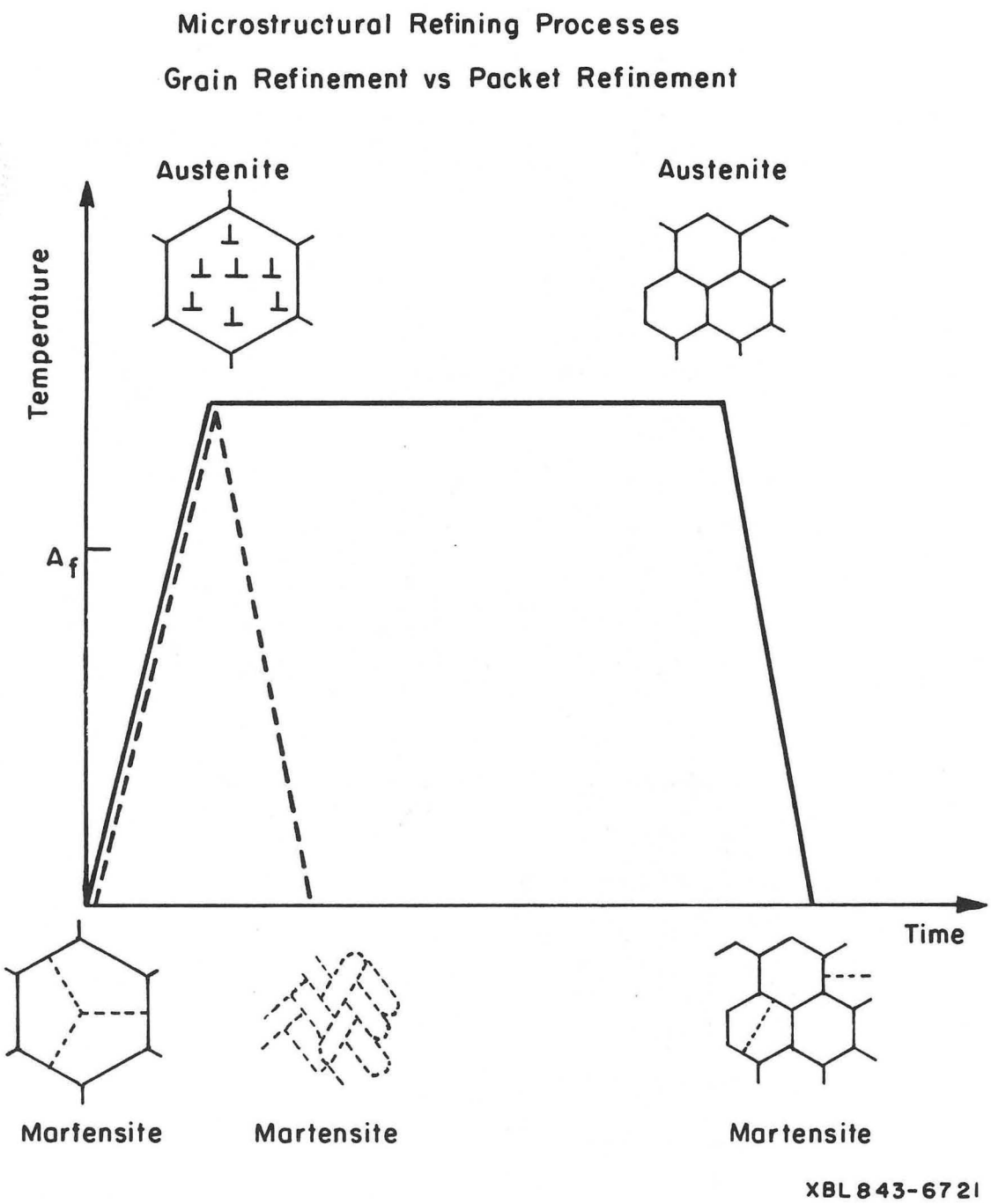

10. Diagram showing the result of austenite reversion with "step" and "spike" thermal profiles.

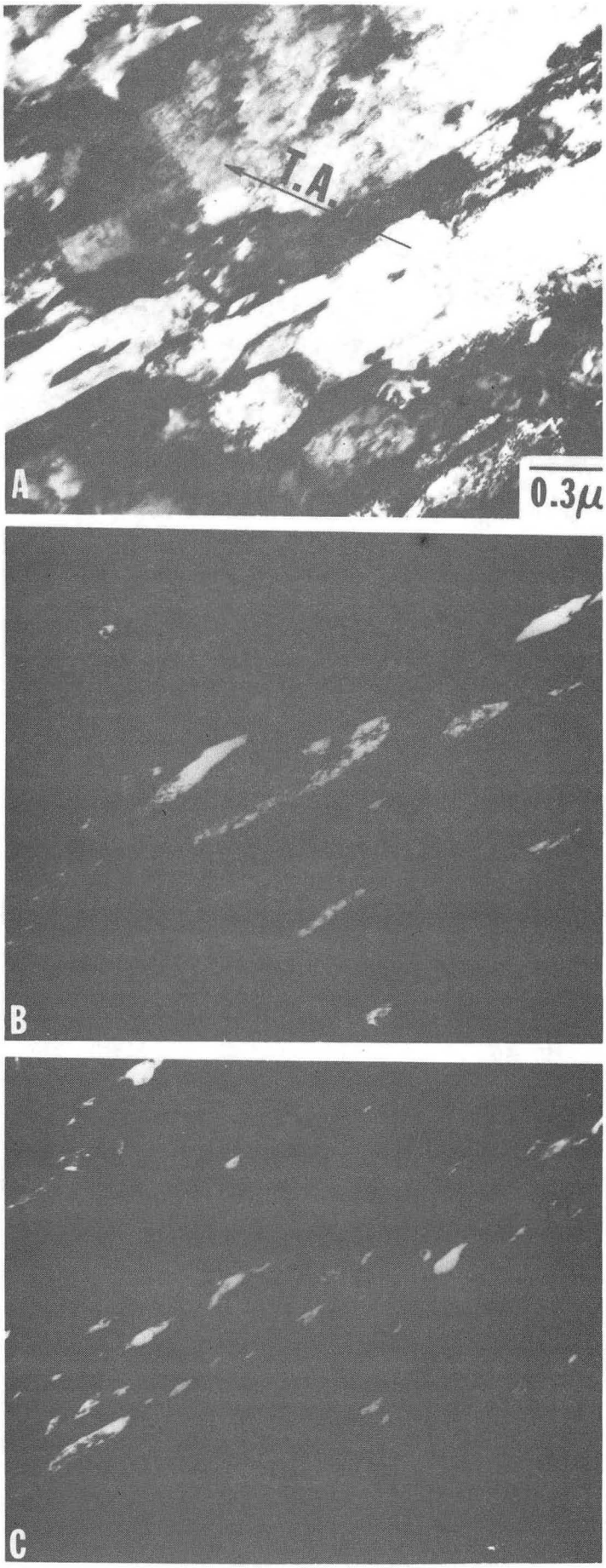

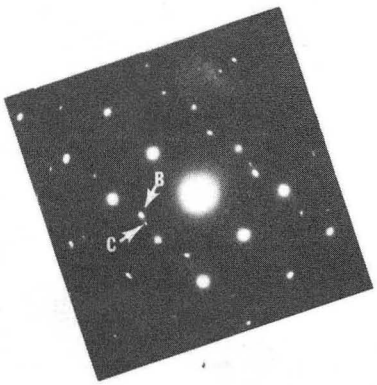

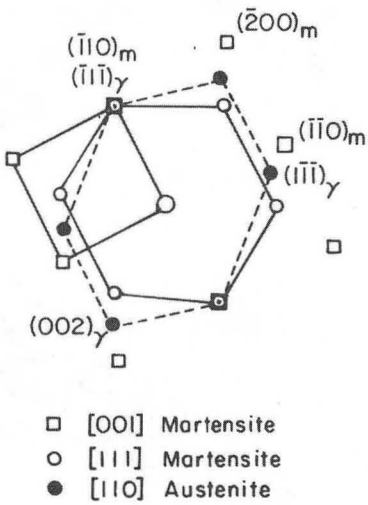

11. Transmission electron micrograph of 9Ni steel in the QT condition after 3% strain: (a) bright field;(b) dark field micrograph of martensite from mechanically transformed austenite; (c) dark field micrograph of remaining austenite. The variant of the fresh martensite differs from that of the surrounding packet.

XBB 790=13860

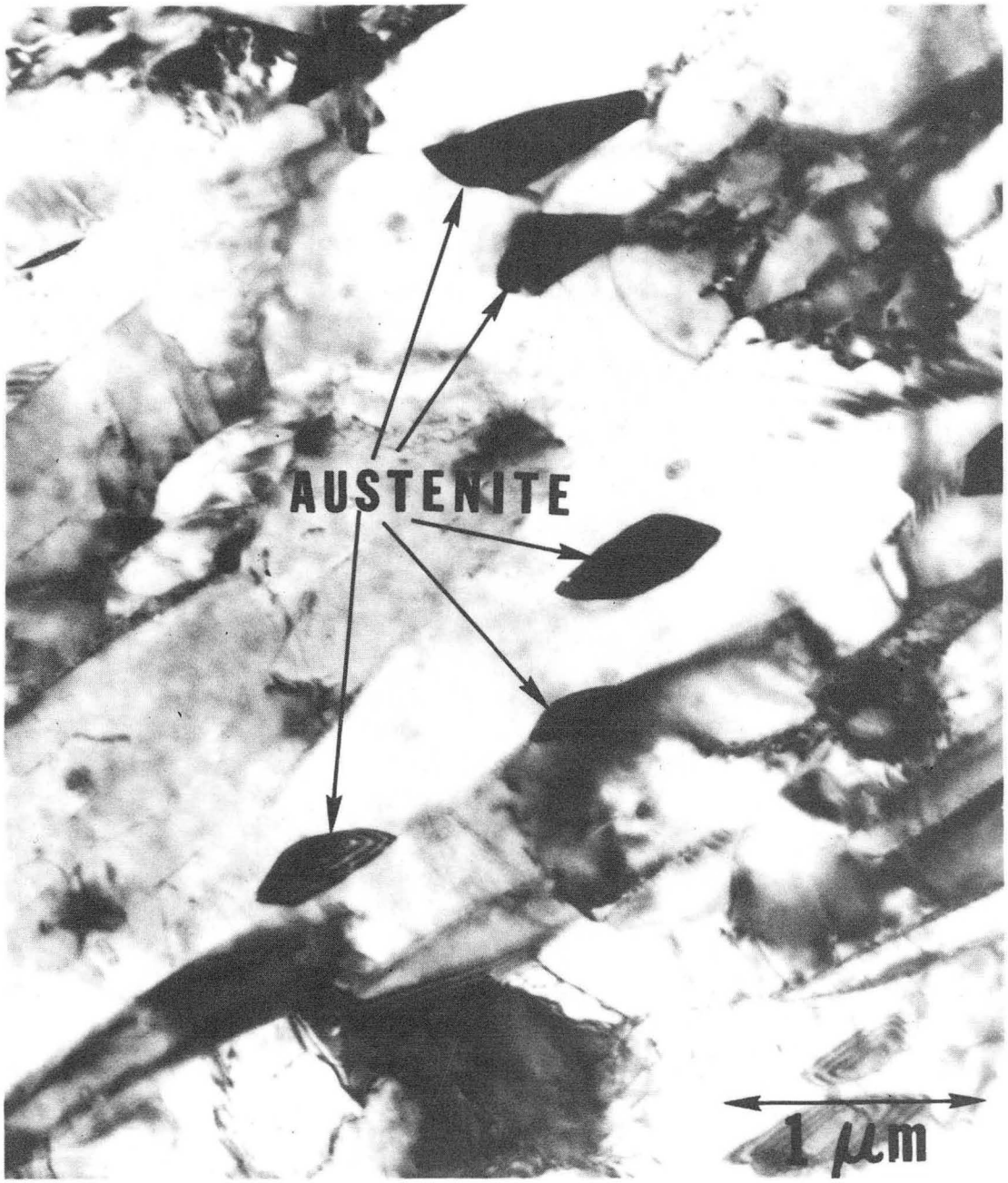

XBB 799-12338

12. Transmission electron micrograph of 5.5Ni steel after tempering at 600°C for 100 hours. The widely separated stable austenite islands are indicated by arrows.

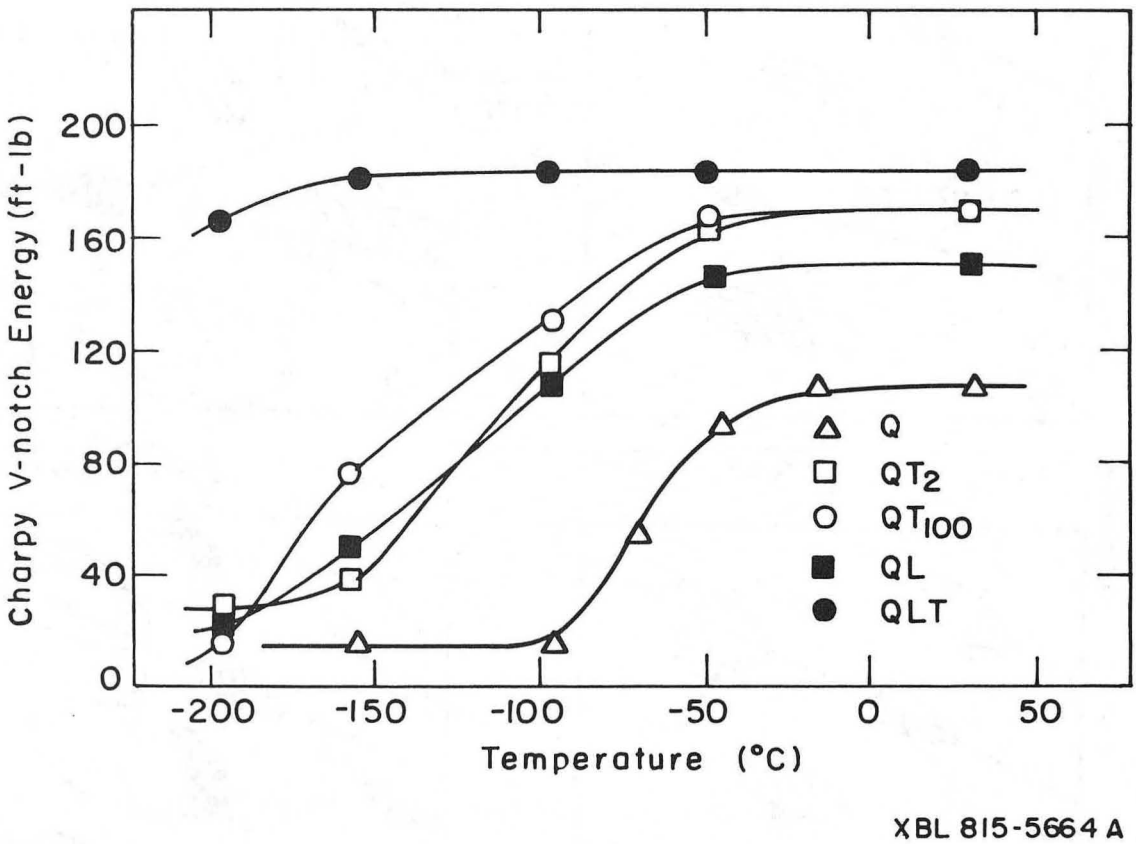

13. Ductile-brittle transition behavior of 5.5Ni steel in the as-quenched (Q), quench-and-tempered (QT^2: 2 hrs., QT^{100}: 100 hrs.), QL, and QLT conditions.

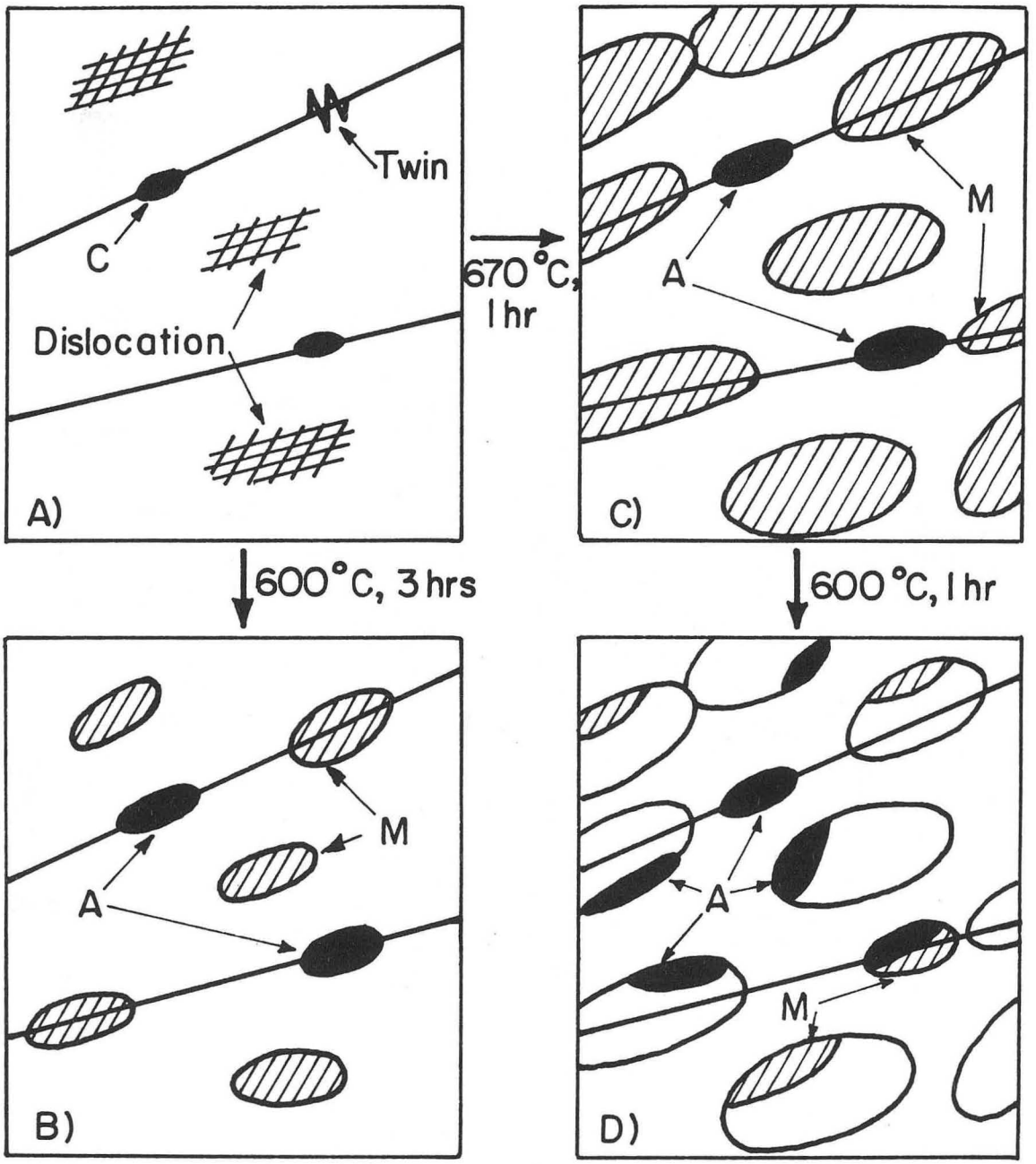

XBL 7910-7191

14. Illustration of the transformation sequence during the QT and QLT treatments of 5.5Ni steel.

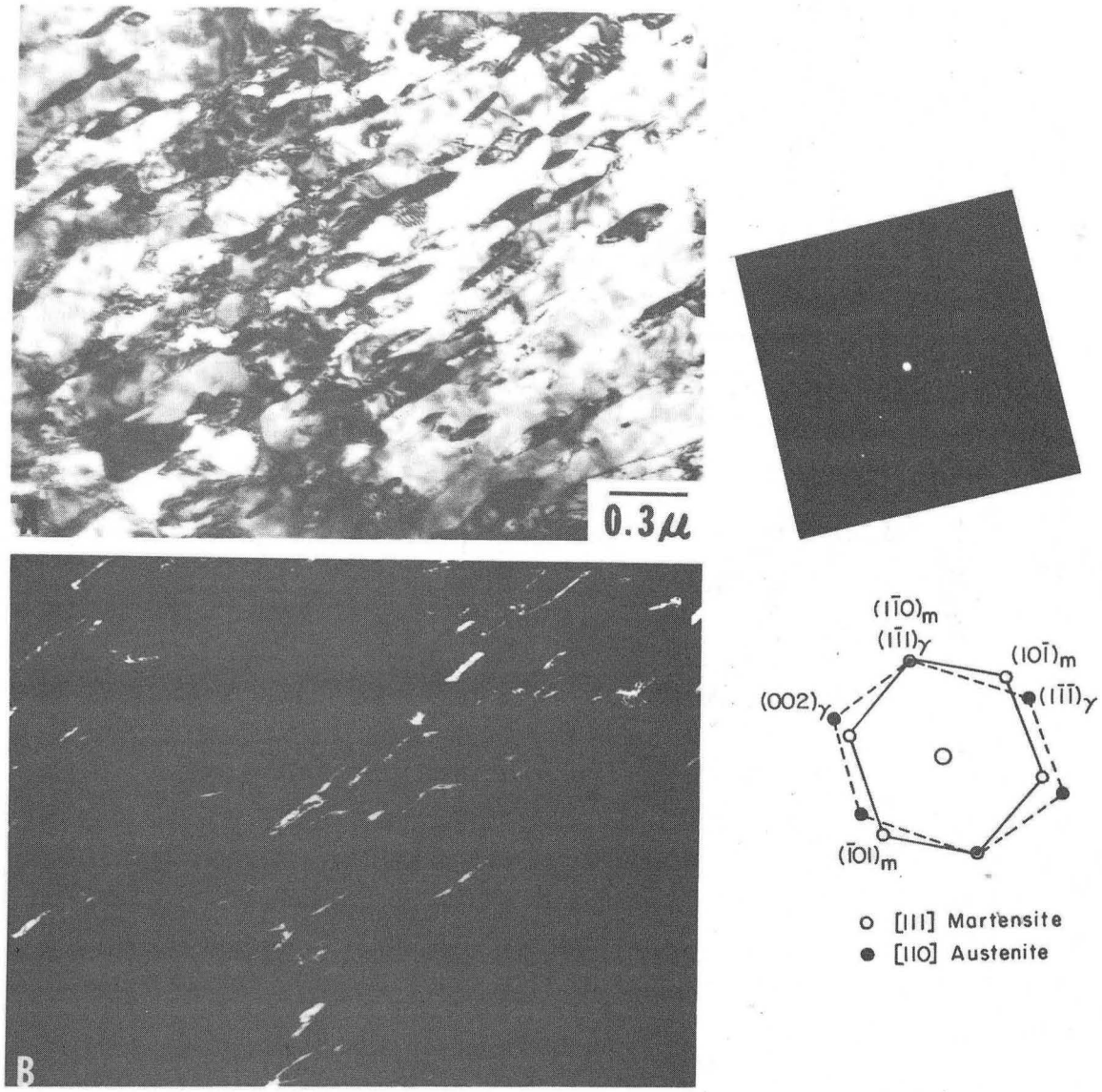

XBB 790-13858

15. Transmission electron micrographs of 5.5Ni steel in the QLT condition. The dark field micrograph shows a dense distribution of precipitated austenite.

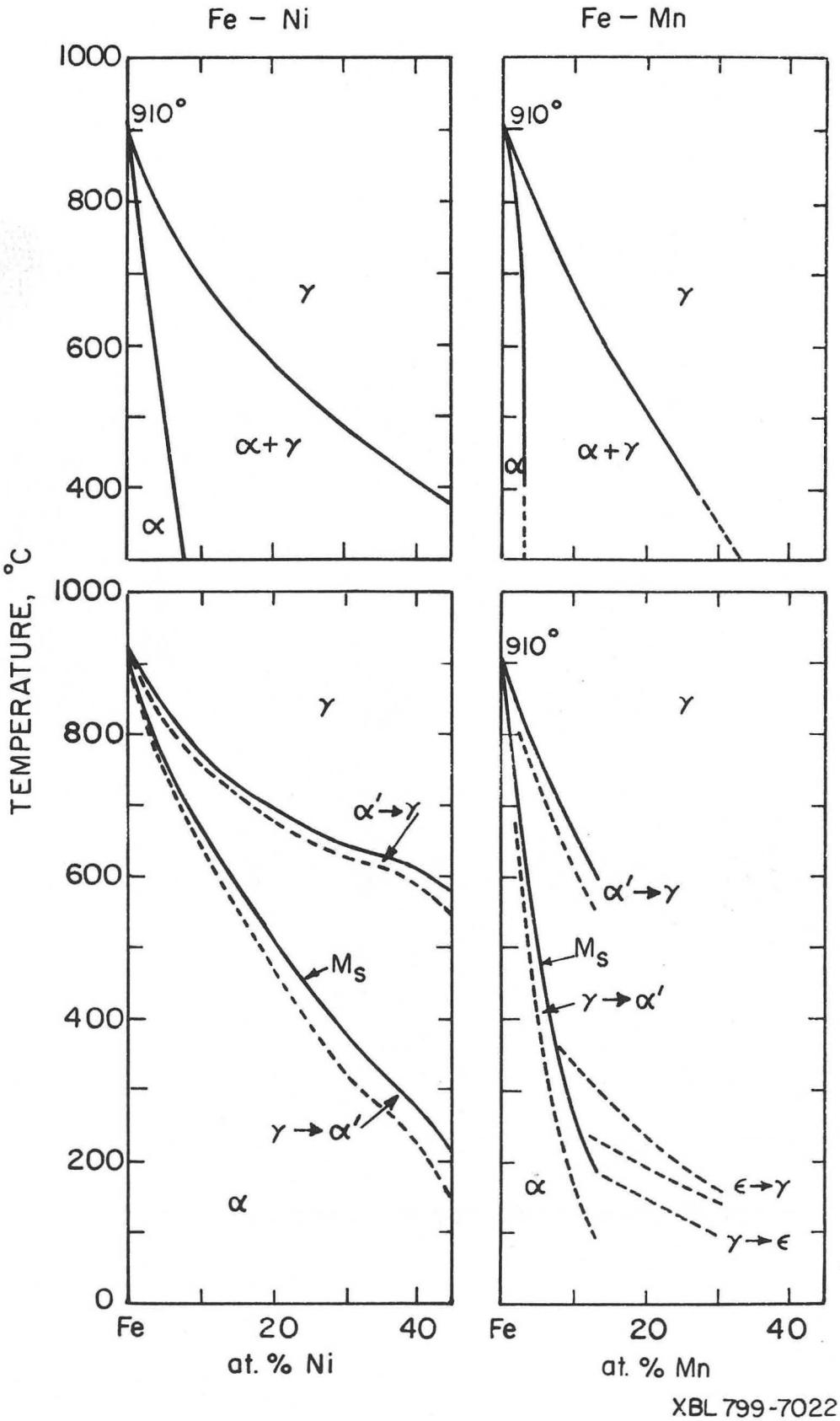

16. Comparison of the Fe-rich sections of the equilibrium and kinetic diagrams (water quench) for the Fe-Ni and Fe-Mn systems.

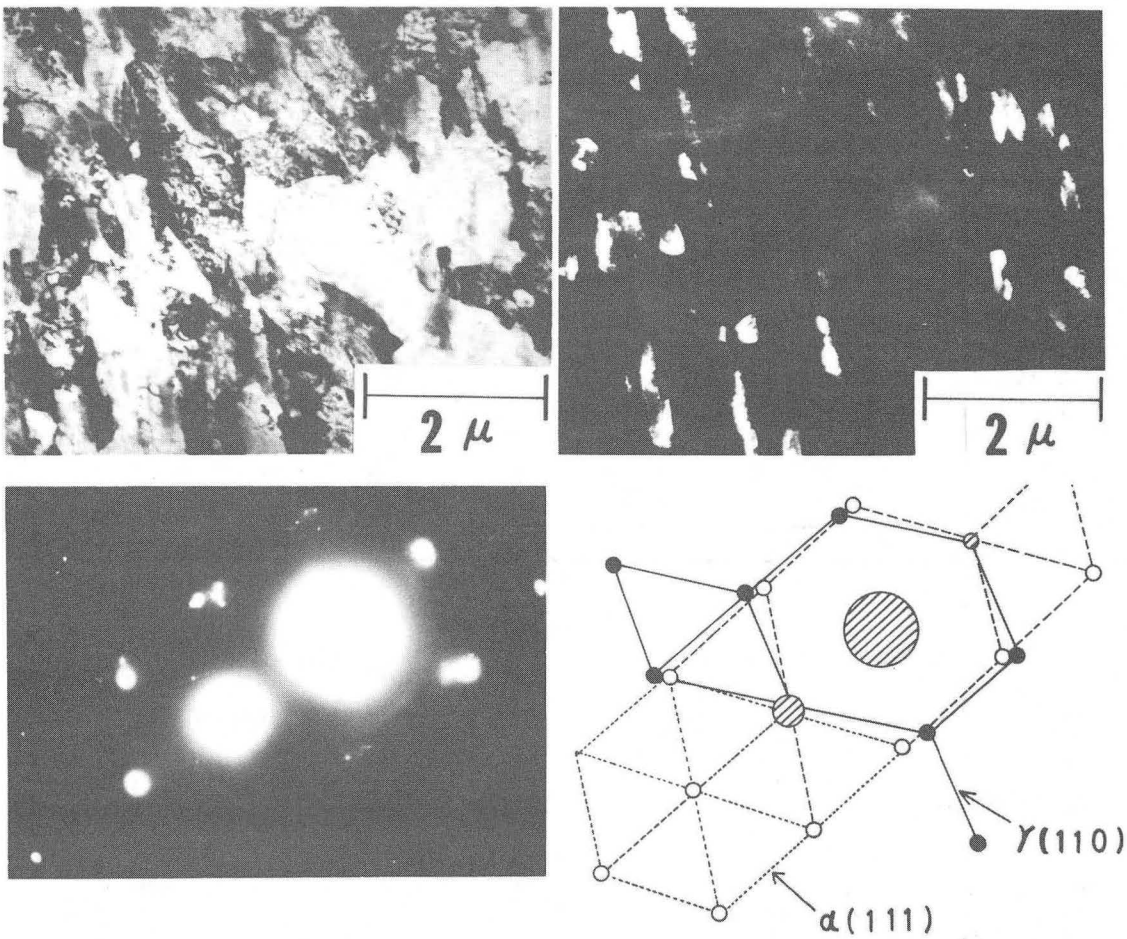

XBB 792-1994A

17. Transmission electron micrographs showing the microstructure and austenite precipitation in Fe-5Mn in the 2BT condition.

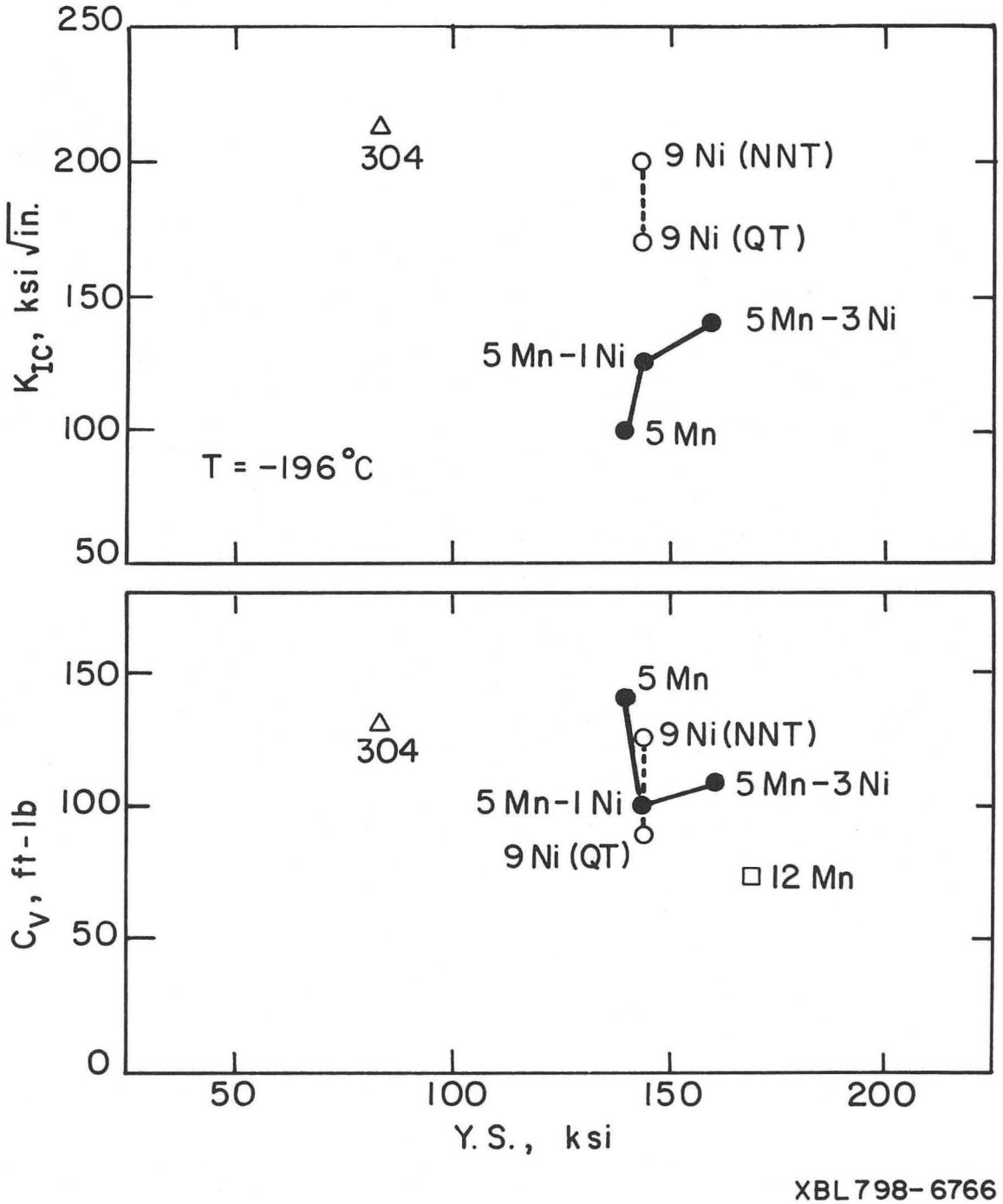

XBL798-6766

18. Comparative plot of the plane strain fracture toughness and Charpy impact energy at 77K for Fe-5Mn, Fe-5Mn-(1-3)Ni, 304 stainless steel, 9Ni steel in two heat treatments, and boron-modified Fe-12Mn [8].

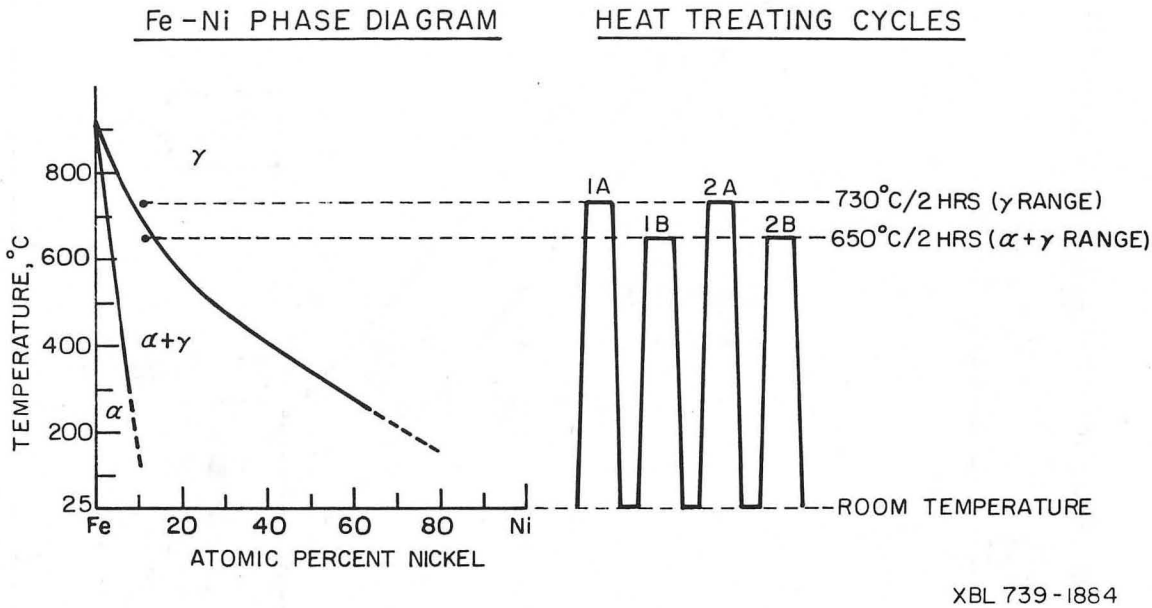

19. Schematic diagram of the 2B heat treatment of Fe-12Ni-0.25Ti.

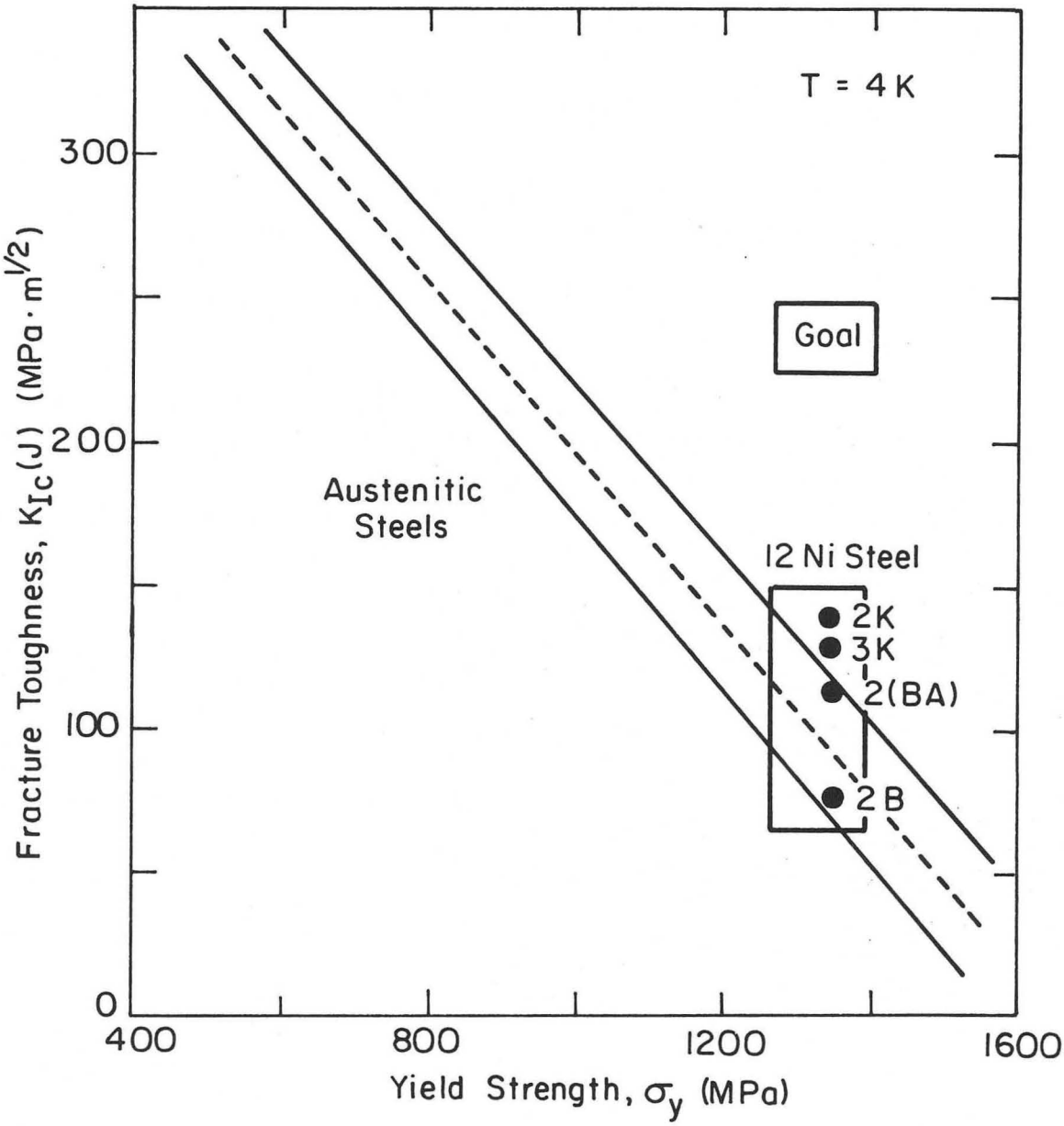

XBL 836-5849

20. The 4K strength-toughness combinations of Fe-12Ni-0.25Ti in various heat treatment conditions. The diagonal band is the trend line for conventional austenitic stainless steels. The "goal" is the "JAERI box", the strength-toughness targets for the Japanese fusion program.

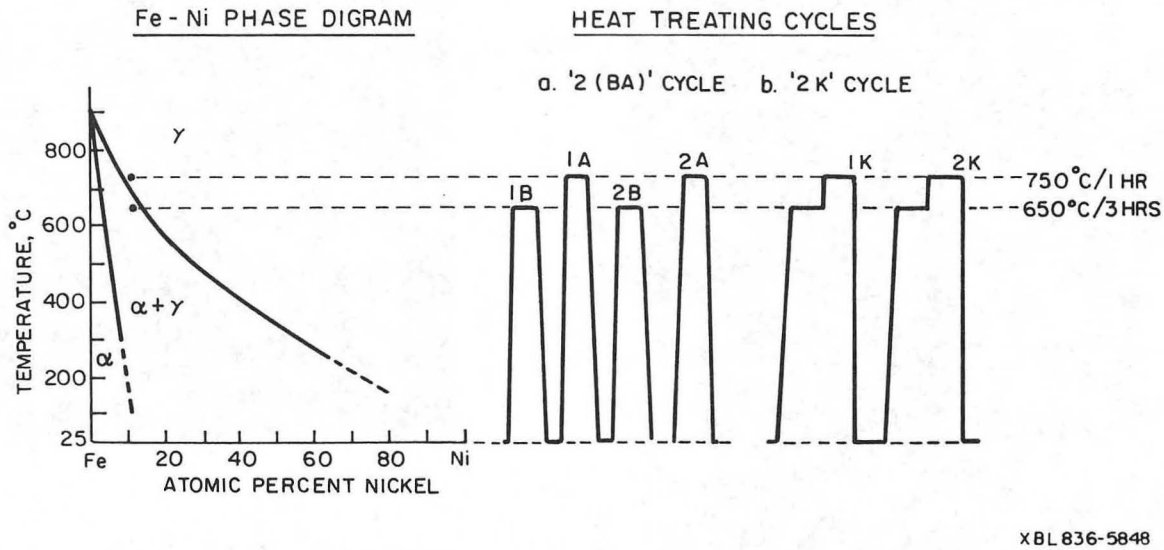

21. Modified thermal cycling treatments used in processing Fe-12Ni-0.25Ti for toughness at 4K.

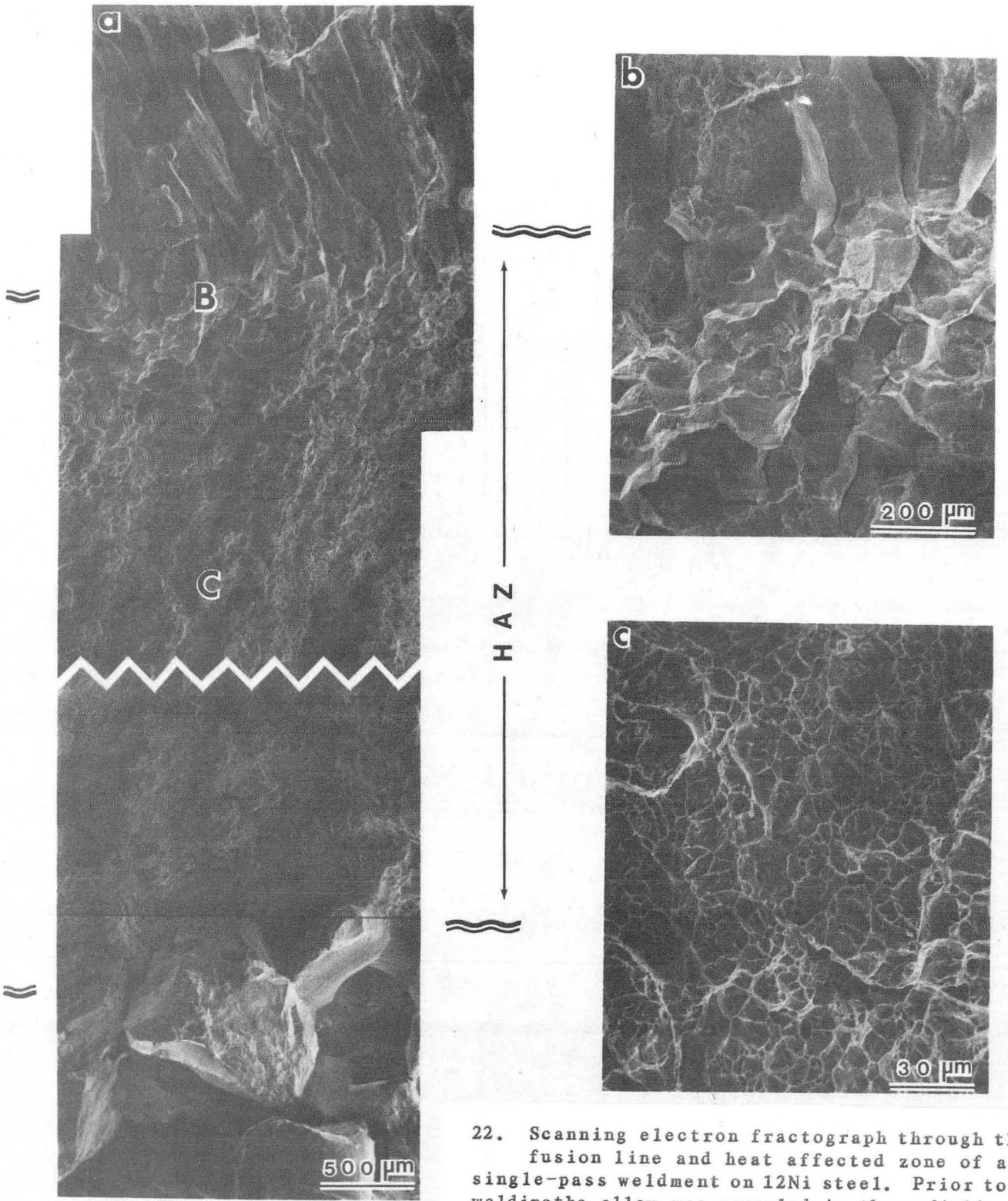

XBB 845-3296

22. Scanning electron fractograph through the fusion line and heat affected zone of a single-pass weldment on 12Ni steel. Prior to weldingthe alloy was annealed in the γ field to producea large starting grain size. After welding it was embrittled at 450°C and then hydrogen-charged before fracture at 77K to promote intergranular fracture.

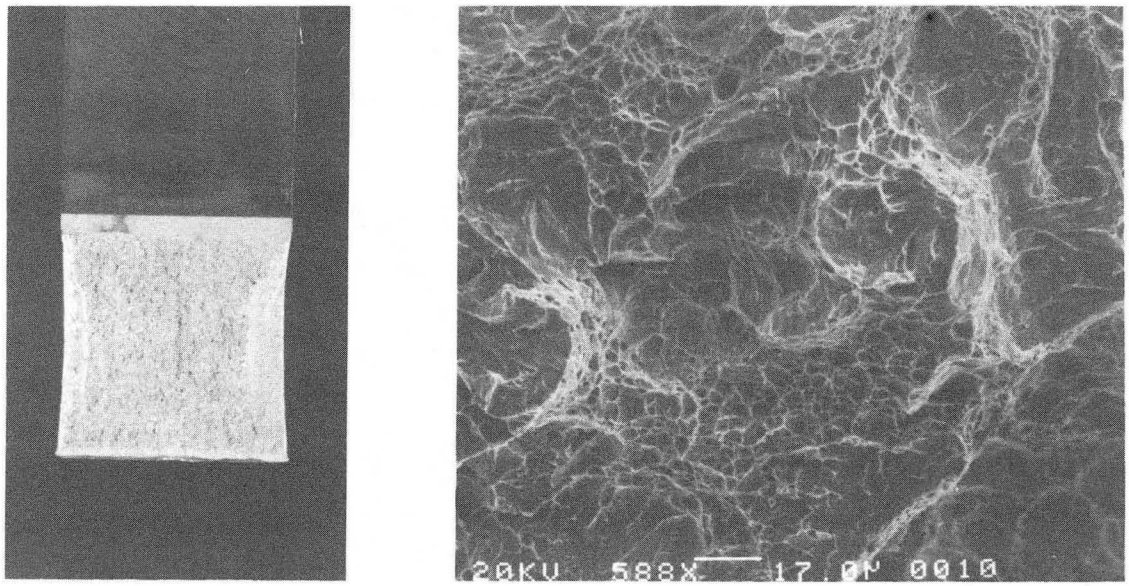

XBB 845-3981

23. Macrograph and scanning electron fractograph of an 11Ni compact tension fracture toughness specimen that was made by multi-pass GTA welding and broken at 4K. The fractograph shows a ductile fracture mode.

This report was done with support from the Department of Energy. Any conclusions or opinions expressed in this report represent solely those of the author(s) and not necessarily those of The Regents of the University of California, the Lawrence Berkeley Laboratory or the Department of Energy.

Reference to a company or product name does not imply approval or recommendation of the product by the University of California or the U.S. Department of Energy to the exclusion of others that may be suitable.

LAWRENCE BERKELEY LABORATORY
TECHNICAL INFORMATION DEPARTMENT
UNIVERSITY OF CALIFORNIA
BERKELEY, CALIFORNIA 94720